THE SPATIAL CROSS-CORRELATION COEFFICIENT AS AN ULTRASONIC DETECTION STATISTIC

A Thesis presented to
the Faculty of the Graduate School
at the University of Missouri – Columbia

In Partial Fulfillment
of the Requirements for the Degree

Master of Science

By
RAINA CEPEL

Dr. K. C. Ho & Dr. Steven P. Neal Thesis Supervisors

December 2007

The undersigned, appointed by the dean of the Graduate School, have examined the thesis entitled

THE SPATIAL CROSS-CORRELATION COEFFICIENT AS AN ULTRASONIC DETECTION STATISTIC

presented by Raina Cepel,

a candidate for the degree of master of science,

and hereby certify that, in their opinion, it is worthy of acceptance.

Dr. K. C. Ho

Dr. Zhihai He

Dr. Steven P. Neal

ACKNOWLEDGEMENTS

Firstly, I am very grateful to have worked with Dr. Steven P. Neal. He has been a good friend and a wonderful mentor over the years we have worked together and I am lucky to have had the opportunity to know him. I will take many of the lessons he has taught me into the rest of my professional career.

I am also grateful to Dr. K. C. Ho for his able insight into this work. Additional thanks go to the other professors I have worked with on this project: Dr. Evan J. Boote, Dr. Lori Thombs, Dr. Terrence P. Lerch, and Dr. Zhihai He.

I would like to thank my husband for always being there for me through life and supporting my education. His comfort and support has been a great help to me, both personally and scholastically.

Finally, I would like to thank my parents, Dr. Reed & Lorraine Olsen for always expecting nothing less than the very best from me.

THE SPATIAL CROSS-CORRELATION COEFFICIENT AS AN ULTRASONIC DETECTION STATISTIC

RAINA CEPEL

Dr. K. C. Ho & Dr. Steven P. Neal - Thesis Supervisors

ABSTRACT

In ultrasonics, image formation and detection are most commonly based on signal amplitude. Matched filtering is an amplitude independent approach, but requires accurate template estimation. In this work, we introduce the use of the spatial cross-correlation coefficient as an additional detection statistic. The correlation coefficients are calculated between A-scans digitized at adjacent measurement positions and can be formed into images that are similar to C-scan images. We also describe an approach for generating simulated acoustic noise with a spatial correlation coefficient distribution and maximum extreme value (MEV) distribution which matches those distributions for measured acoustic noise. Using the simulated acoustic noise, grain noise and noise-corrupted flaw signals are simulated under varying conditions to compare performance. The spatial cross correlation approach is found to outperform gated peak detection at low signal to noise ratios. When the *a priori* flaw signal prediction is inadequate, the correlation approach also outperforms matched filtering. Techniques to maximize the efficacy of the spatial cross correlation approach are suggested.

TABLE OF CONTENTS

LIST OF FIGURES

NOMENCLATURE

$a(i,j,t)$	uncorrelated random acoustic noise
$b_C(i,j)$	column scale factor
$b_R(i,j)$	row scale factor
E_x	sum of square errors between simulated and measured A-scans
$F_k(f)$	filter
FPF	false positive fraction
h_c	histogram for simulated noise
h_m	histogram for measured noise
$h_i(t)$	input pulse
$h_i^m(t)$	matched filter input pulse template
i	lateral x position
j	lateral y position
k	number of bins in histogram
N	total number of A-scans in a row
$n_i(t)$	noise at position i
M	total number of A-scans in a column
m_{mev}	mean measured maximum extreme value
$P(\rho(i))$	probability distribution function of correlation coefficients
$r_i(t)$	impulse response of flaw at position i
$s_i(t)$	signal from flaw at position i
$s_i^m(t)$	matched filter estimate of signal from flaw at position i
T	total number of points of time window
TPF	true positive fraction
t	time
t_i	initial time (for windowing)
t_f	final time (for windowing)
$\lvert X_m(f)\rvert$	average magnitude spectrum of measured A-scans
$\lvert X_k(f)\rvert$	average magnitude spectrum of simulated A-scans
$\lvert X_m(f)\rvert^2$	average power spectral density function estimate of A-scans
$x(i,j,t)$	grain noise signals
$y(i,j,t)$	flaw signals

$z(i,j,t)$	received signals (A-scans), flaw plus grain noise
α_c	similarity between two noise corrupted flaw signals
α_m	similarity between actual signal and matched filter estimate of signal
α_n	similarity between noise and matched filter estimate of signal
α_{nn}	similarity between two adjacent noise signals
β_c	maximum value of correlation output
β_m	maximum value of matched filter output
δ_c	column spatial shift parameter
δ_r	row spatial shift parameter
ε_x	acceptable sum of square errors
$\tau(i,j)$	lag or temporal shift between two adjacent signals
$\lvert\tau\rvert_{\max}$	maximum value of the lag
σ_a	standard deviation of maximum extreme value of uncorrelated random acoustic noise
σ_x	standard deviation of maximum extreme value of received signals
$\rho = \rho(i,j,t_i,t_f,\tau,\delta_r,\delta_c)$	correlation coefficients
$\tilde{\rho}_c(i,j)$	desired column correlation coefficients
$\tilde{\rho}_r(i,j)$	desired row correlation coefficients
$\overline{\rho}_c(i,j)$	actual column correlation coefficients
$\overline{\rho}_r(i,j)$	actual column correlation coefficients
χ^2	chi-squared error

CHAPTER 1
INTRODUCTION

Gated-peak detection, a typical ultrasonic detection in nondestructive evaluation (NDE), is amplitude based. The statistic used for this approach is either the maximum absolute value or the maximum peak to peak value of a voltage versus time signal, called an A-scan. An image of these values plotted versus their corresponding lateral spatial positions is called a C-scan. The C-scan image represents a starting point for the application of image processing techniques to identify defects as spatial regions of high or low amplitude relative to the background amplitude-based noise. A weakness of amplitude based approaches is their direct and inherent sensitivity to non-defect related amplitude changes associated with the measurement system or material sample, thus efficacy at low SNR is poor.

Matched filtering is another detection technique [1,2] that filters each received signal with a template that is chosen by the user to be the best match to the expected flaw signal. In effect, matched filtering correlates each measured A-scan with the template. This approach is amplitude independent and as such has the capability to be effective at low SNR, but only when an accurate prediction of the flaw signal is used. In instances where the template is significantly different from the flaw signals, the performance of matched filtering degrades. Previous work on the use of matched filter for ultrasonic defect detection by Xin et al. [3], Chiou et al. [4], and Srinivasan et al. [5] addresses the difficulties in estimating the template along with the use of model-based approaches for template estimation.

In this work, we focus on a complementary technique which relies on the cross-correlations between adjacent A-scans [6,7] as a basis for detection [8,9]. Spatial cross-

correlation coefficient images are introduced as signal amplitude independent approach for visualizing the similarity in measured A-scans. Correlation images are created using the same A-scans which form the basis of C-scan images. In either case, the process begins with measured A-scans written into a three-dimensional array with the rows and columns of the array registered with the measurement locations and time being the third dimension. Formation of a correlation image is more complicated than formation of a C-scan image, but the basic approach is the same: establish a time gate, calculate the correlation coefficient between adjacent A-scans which were written into the three-dimensional array, write the correlations into a two-dimensional array, and form a correlation image based on the correlations [9]. Correlation images represent a complimentary starting point for the application of image processing techniques to identify defects as regions of high or low correlation relative to the background noise.

Simulation studies are utilized to quantify the usefulness of the spatial cross-correlation as an ultrasonic detection technique. Simulated A-scans typically include a target signal (e.g., a flaw or weld plane signal) plus noise. In some cases, the degree of average correlation between adjacent A-scans can have a significant influence on detection [10-14]. Therefore, to accurately simulate signals, they must be constructed with correlated grain noise. Uncorrelated grain noise is easily generated using a normal random number generator with filtering used to achieve the desired frequency content. To create correlated noise, each noise signal is created as a weighted sum of a random signal and the signals in adjacent measurement locations.

With accurate simulated grain noise, noise-corrupted flaw signals can be created under varying conditions in order to quantitatively compare the performance of the spatial

cross-correlation method to the gated peak-detection and matched filtering approaches. This will aid decisions about when the spatial cross-correlation detection statistic should be used in addition to gated-peak detection or matched filtering.

The results of this work are presented in the next three chapters, each of which is written as a self-contained paper. Chapter 2 was published in *IEEE Transactions on Ultrasonic & Ferroelectric Frequency Control* [15] and describes the process of correlation image formation in more detail, including complications which arise from initial alignment of A-scans, local alignment of signals, skipping signal measurement positions, and image formation using matrices with blank elements. It also shows examples of correlation images with complimentary C-scan images, and qualitatively compares the spatial cross-correlation coefficient to matched filtering.

Chapter 3 was published in *The Journal of Nondestructive Evaluation* [16] and describes the approach for generating simulated acoustic noise with a correlation coefficient distribution and maximum extreme value (MEV) distribution (i.e, the gated peak-value distribution) which matches the distributions determined for measured acoustic noise. Each correlated noise signal is created as a weighted sum of a random signal and the signals in adjacent measurement locations, with an iterative procedure for determining the weights resulting in a set of spatially correlated noise signals.

Chapter 4, which has not yet been submitted for publication, noise-corrupted flaw signals are created under varying conditions in order to quantitatively compare the performance of the spatial cross-correlation method to the gated peak-detection and matched filtering approaches. For each set of conditions, a receiver operating characteristic curve is calculated for each detection statistic and the area under the curve is used as a basis for

comparing each detection approach. Some conclusions are made about under which circumstances the use of spatial cross-correlation should be considered, and recommendations are made to aid in maximizing the efficacy of this detection approach given certain invariant experimental conditions

References

1. S. M. Kay, Fundamentals of Statistical Signal Processing Volume II Detection Theory. Prentice-Hall, Upper Saddle River, NJ, 1998.

2. A. D. Whalen, Detection of Signals in Noise, New York: Academic Press, 1971.

3. J. Q. Xin, K. D. Donohue, and N. M. Bilgutay, "Filter design for ultrasonic flaw echo detection in large-grained material", *Review of Progress in Quantitative Nondestructive Evaluation*, Vol. 10A, edited by D. E. Chimenti and D. O. Thompson, Plenum Press, New York, 1991, pp. 725-731.

4. C. P. Chiou, R. B. Thompson, and L. W. Schmerr, "Model-based signal processing techniques for ultrasonic flaw detection: simulation studies", *Review of Progress in Quantitative Nondestructive Evaluation*, Vol. 12A, edited by D. E. Chimenti and D. O. Thompson, Plenum Press, New York, 1993, pp. 703-710.

5. K. Srinivasan, C. Chiou, and R. B. Thompson, "Ultrasonic flaw detection using signal matching techniques", *Review of Progress in Quantitative Nondestructive Evaluation*, Vol. 14A, edited by D. E. Chimenti and D. O. Thompson, Plenum Press, New York, 1993, pp. 711-718.

6. J. S. Bendat and A. G. Piersol, *Engineering Applications of Correlation and Spectral Analysis*, J. Wiley, New York, p. 46, 1993.

7. W. F. Walker, "The significance of correlation in ultrasound signal processing", *Proc. SPIE Vol. 4325, Medical Imaging: Ultrasonic Imaging and Signal Processing*, edited by Michael F. Insana and K. Kirk Shung, 2001, pp. 159-171.

8. B. A. Rinker, E. E. Jamieson, J. A. Samayoa, T. G. Abeln, T. P. Lerch, and S. P. Neal, "Detection of weak interface signals for same material bond/weld inspection", *Review of Progress in Quantitative Nondestructive Evaluation*, Vol. 22B, edited by D. E. Chimenti and D. O. Thompson, AIP, Melville, 2003, pp. 1080-1087.

9. R. Cepel, K. C. Ho, B. A. Rinker, D. D. Palmer, Jr., and S. P. Neal, "Ultrasonic detection using correlation images", *Review of Progress in Quantitative Nondestructive*

Evaluation, Vol. 26, edited by D. E. Chimenti and D. O. Thompson, AIP, Melville, 2007, (in press).

10. R. B. Thompson, L. Yu, and F. J. Margetan, "A formal theory for the spatial correlation of backscattered ultrasonic grain noise", *Review of Progress in Quantitative Nondestructive Evaluation*, Vol. 24, edited by D. E. Chimenti and D. O. Thompson, AIP, Melville, 2005, pp. 1292-1299.

11. F. J. Margetan, E. Nieters, L. Brasche, L. Yu, A. Degtyar, H. Wasan, M. Keller, and A. Kinney, "Fundamental Studies of Titanium Forging Materials - Engine Titanium Consortium II", FAA William J. Hughes Technical Center, Atlantic City, N. J., Report number DOT/FAA/AR-05/22 (June 2005).

12. A. Dogandzic and N. Eua-Anant, "Defect detection in correlated noise", *Review of Progress in Quantitative Nondestructive Evaluation*, Vol. 23A, edited by D. E. Chimenti and D. O. Thompson, AIP, Melville, 2004, pp. 628-635.

13. W. F. Walker, "The significance of correlation in ultrasound signal processing", *Proc. SPIE Vol. 4325, Medical Imaging: Ultrasonic Imaging and Signal Processing*, edited by Michael F. Insana and K. Kirk Shung, 2001, pp. 159-171.

14. J. S. Bendat and A. G. Piersol, *Engineering Applications of Correlation and Spectral Analysis*, J. Wiley, New York, p. 46, 1993.

15. R. Cepel, K. C. Ho, B. A. Rinker, D. D. Palmer, Jr., T. P. Lerch, and S. P. Neal, "Spatial correlation coefficient images for ultrasound detection", *IEEE Trans. Ultrason. Ferroelectr. Freq. Control* (in press).

16. R. Cepel, L. Thombs, K. C. Ho, and S. P. Neal, "Statistical analysis and computer generation of spatially correlated acoustic noise", *J. Nondestr. Eval*., (in press).

CHAPTER 2
SPATIAL CORRELATION COEFFICIENT IMAGES FOR ULTRASONIC DETECTION

by

Raina Cepel, K. C. Ho, Brett A. Rinker, Donald D. Palmer, Jr., Terrence P. Lerch, and

Steven P. Neal

Abstract:

In ultrasonics, image formation and detection are generally based on signal amplitude. In this paper, we introduce correlation coefficient images as a signal amplitude independent approach for image formation. The correlation coefficients are calculated between A-scans digitized at adjacent measurement positions. In these images, defects are revealed as regions of high or low correlation relative to the background correlations associated with noise. Correlation coefficient and C-scan images are shown to demonstrate flat-bottom-hole detection in a stainless steel annular ring and crack detection in an aluminum aircraft structure.

I. Introduction

Typical ultrasonic detection in nondestructive evaluation (NDE) is amplitude based. C-scan images are used to display peak-amplitudes throughout a scan. The C-scan image represents a starting point for the application of image processing techniques to identify defects as regions of high or low amplitude relative to the background amplitude-based noise. A weakness of amplitude based approaches is their direct and inherent sensitivity to non-defect related amplitude changes associated with the measurement system or material sample. In this paper, we focus on a complementary image formation approach which relies on the correlations between adjacent A-scans [1,2] as a basis for detection [3,4]. Correlation coefficient images are introduced as signal amplitude independent approach for visualizing the similarity in measured A-scans. Correlation images represent a complimentary starting point for the application of image processing techniques to identify defects as regions of high or low correlation relative to the background noise.

Correlation images are created using the same A-scans which form the basis of C-scan images. In either case, the process begins with measured A-scans written into a three-dimensional array with the rows and columns of the array registered with the measurement locations and time being the third dimension. Formation of a correlation image is more complicated than formation of a C-scan image, but the basic approach is the same: establish a time gate, calculate the correlation coefficient between adjacent A-scans which were written into the three-dimensional array, write the correlations into a two-dimensional array, and form a correlation image based on the correlations [4]. As will be discussed, complications arise from initial alignment of A-scans, local alignment of signals, skipping signal measurement positions, and image formation using matrices with blank elements.

The correlation approach addressed here contains at least an element of matched filtering [5,6]. As applied to defect detection using ultrasonics, implementation of a matched filter is comparable to calculating the cross-correlation between the expected defect signal, denoted the filter's impulse response or template, and each windowed A-scan [7-12]. An image of matched filter correlations could then be constructed. The efficacy of this approach as applied to ultrasonics is directly related to the quality of the template; in essence, the efficacy is controlled by the operator's ability to predict the signal distortion caused by scattering at an unknown defect. Specifically as related to defect detection in ultrasonics, Xin et al. [7], Chiou et al. [8], and Srinivasan et al. [9] address the difficulties in estimating the template along with the use of model-based approaches for template estimation. Eriksson et al. [10] address the problem of correlation-based time-of-flight estimation when the signals have undergone unknown non-linear distortions. In the correlation approach, each signal is correlated with its nearest neighbors, with resultant correlations used as a basis for correlation image formation. In essence, each gated A-scan is taken to be a template for application of matched filtering to neighboring A-scans. A more detailed comparison of the matched filter and correlation approaches is pursued below.

The remainder of this paper deals with the details associated with correlation image formation including measurement procedures, correlation calculations, and image formation alternatives. Examples of correlation images are presented based on measured A-scans. Companion C-scan images are presented for comparison purposes. The paper closes with a summary and discussion section.

II. Ultrasonic measurements

A-scans were measured in an immersion mode using two samples: a stainless steel annular ring with nominal inside and outside diameters of 40 mm and 70 mm, respectively; and an aluminum sample fabricated to represent an aircraft structure. The annular ring sample was machined to add five equal-depth flat bottom holes. A Panametrics 15 MHz, ½" diameter, 6" focal length transducer was used in a polar scan at normal incidence on the annular sample with 2° between radial scan lines and 0.762 mm between circumferential scan lines. Data from the annular sample was used to show polar correlation images and to present correlation images for flat-bottom-hole signals within grain noise. The aluminum sample was comprised of two aluminum plates fastened together with a sealant between the two plates. Electric discharge machined (EDM) notches of various lengths were machined to extend radially from selected fastener holes. For the aluminum sample, oblique incidence pitch-catch measurements were made using a pair of Panametrics 10 MHz, ½" diameter transducers, one flat and one with a focal length of 3". Transducers were arranged 5° from normal. The aluminum sample with simulated cracks was used to demonstrate the use of correlation images for the detection of cracks based on lack of correlation in transmitted signals.

III. The correlation approach and formation of correlation images

A. Model formulation and relationship to the matched filter

In this section, enough detail is given to provide a framework for introduction of the correlation approach and to facilitate a first order comparison between the correlation approach and a matched filter approach. We start by stating a convolution-based model for a backscattered signal, $x_i(t)$, measured at the i^{th} measurement position in a line scan:

$$\begin{aligned} x_i(t) &= h_i(t) * r_i(t) + n_i(t) \\ &= \quad s_i(t) \quad + n_i(t) \end{aligned} \tag{1}$$

where $h_i(t)$ is a copy of the input pulse that includes all measurement system and material effects other than scattering at the flaw, $r_i(t)$ is the impulse response function for the flaw (i.e., the inverse Fourier transform of the flaw's scattering amplitude), and the noise, $n_i(t)$, is assumed to be white in order to simplify the development. The noise-free flaw signal, $s_i(t)$, is a distorted version of $h_i(t)$ with the distortion caused by scattering at the flaw: $s_i(t) = h_i(t) * r_i(t)$.

For a matched filter approach, the impulse response or template of the matched filter could be calculated as the time-reversal of $s_i^m(t) = h_i^m(t) * r_i^m(t)$ [5]. In an ideal case, we have $s_i^m(t) = s_i(t)$. This ideal case is generally unrealizable due to the inherent nature of the problem; that is, the problem of searching for unknown defects with unknown scattering functions [7-10]. To simplify the comparison with the correlation approach, we can write the key relationship driving the matched filter approach using a covariance format as follows:

$$\begin{aligned} \beta_m &= \sum s_i^m(t) x_i(t) = \sum_t s_i^m(t) s_i(t) + \sum_t s_i^m(t) n_i(t) \\ &= \quad \alpha_m \quad + \quad \alpha_n \end{aligned} \tag{2}$$

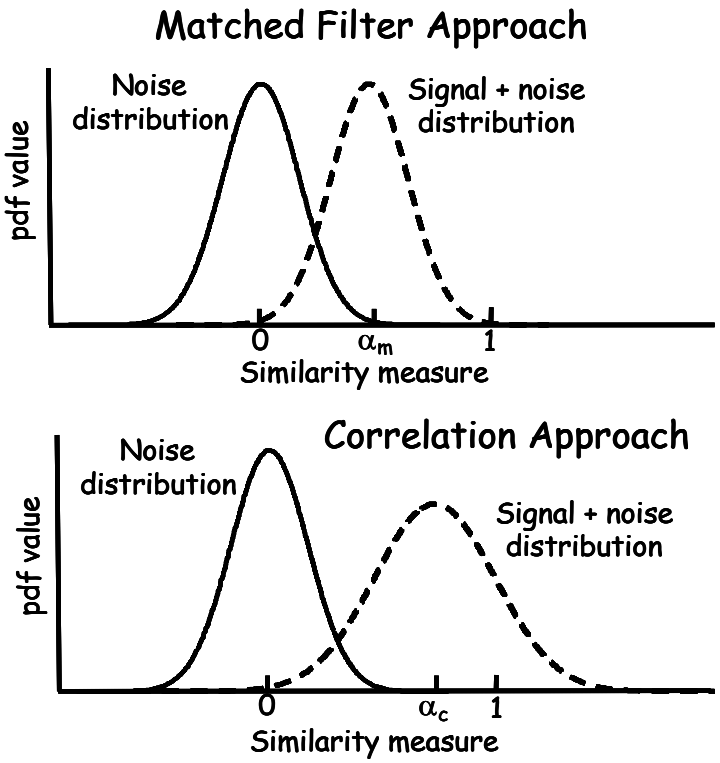

Fig. 1. Representation of noise and signal + noise distributions for: (a) matched filter (upper) and (b) correlation approach (lower).

where for ease of notation, the time delay between $s_i^m(t)$ and $x_i(t)$ has been accounted for and β_m is the maximum value of the matched filter output. Furthermore, we assume that the flaw signals all have unit energy and that all processes are zero mean. A measure of the quality of the matched filter template is given by the similarity in $s_i^m(t)$ and $s_i(t)$ as quantified by α_m. Given the unit energy assumption, $\alpha_m = 1$ for the ideal case where $s_i^m(t) = s_i(t)$. In this simplified development, α_m is taken to be deterministic. Now consider two cases: no flaw signal $\Rightarrow \beta_m = \alpha_n$, resulting in the noise distribution; and flaw signal present $\Rightarrow \beta_m = \alpha_m + \alpha_n$, resulting in the signal + noise distribution. Figure 1(a) shows a representation of the distributions for β_m with and without a signal. Assuming

further that the measurement position spacing is great enough that adjacent noise signals are uncorrelated [13-15], the noise distribution will have zero mean with variance driven solely by α_n. Similarly, the signal + noise distribution will have mean α_m with the same variance as that for the noise distribution. Thinking in terms of a receiver operator characteristic (ROC) analysis, the performance of the filter will be essentially controlled by the amount of overlap between the two distributions. The degree of overlap is controlled by the width of the distributions (which are both controlled by the noise variance) and by the position of the signal + noise distribution (which is controlled by the quality of the template). For the ideal case where the template "matches exactly" the flaw signal, $\alpha_m = 1$, and the matched filter approach reaches its best performance. In practice, $h_i(t)$ may be calculated reasonably well (at least for isotropic materials), $r_i(t)$ is generally difficult to estimate, and $s_i^m(t)$ therefore does not "match well" with $s_i(t)$ [7-10]. As a result, α_m is less than 1, the distribution of β_m moves to the left, and the matched filter performance degrades. Finally, we note that while not typically done in practice, β_m could be used to form a matched filter following the basic concepts described below.

For the correlation approach, the correlation between adjacent signals is calculated. This is in contrast to the matched filter which basically utilizes the correlation between the template and each signal. Continuing with the same development format and with the same simplifying assumptions, we can write a key relationship supporting the correlation approach as follows:

$$\beta_c = \sum_t x_i(t)x_{i+1}(t) = \sum_t \left[s_i(t) + n_i(t)\right]\left[s_{i+1}(t) + n_{i+1}(t)\right]$$

$$= \sum_t s_i(t)s_{i+1}(t) + \sum_t s_i(t)n_{i+1}(t) + \sum_t s_{i+1}(t)n_i(t) + \sum_t n_i(t)n_{i+1}(t) \quad (3)$$

$$= \quad \alpha_c \quad + \quad \alpha_{n1} \quad + \quad \alpha_{n2} \quad + \quad \alpha_{nn}$$

Again, α_c is considered deterministic. For the correlation approach, three cases must be considered: no flaw signal $\Rightarrow \beta_m = \alpha_{nn}$, resulting in the noise distribution; flaw signal present in both signals $\Rightarrow \beta_c = \alpha_c + \alpha_{n1} + \alpha_{n2} + \alpha_{nn}$, resulting in a signal + noise distribution; and a flaw signal in only one signal $\Rightarrow \beta_c = \alpha_c + \alpha_{n1} + \alpha_{nn}$, resulting in a second signal + noise distribution. This last case will exist only at the border of a flaw with one A-scan on the flaw and one missing the flaw; therefore, this case will be ignored for discussion purposes. Figure 1(b) shows a representation of the distributions for β_c with and without a signal. The noise distribution will have zero mean and variance driven only by the variance of α_{nn}. The signal + noise distribution will have mean at α_c, but the variance of distribution will now be driven by the variance of $\alpha_{n1} + \alpha_{n2} + \alpha_{nn}$. As a result of using what is essentially a noise-corrupted template, the correlation approach shows more noise than the matched filter. The overlap in distributions, however, will also be influenced by mean of the signal + noise distribution as represented by α_c.

Given these models, we can state that the rationale behind the correlation approach is that the potential exists for the similarity between flaw signals from adjacent measurement positions to be greater than the similarity between the template and either measured flaw signal; implying that $\alpha_c > \alpha_m$. Even given this rationale, for enhanced performance, the

positive effect of $\alpha_c > \alpha_m$ must overcome the effect of an increase in noise due to the use of, in essence, a noise-corrupted template. Considering the issues behind $\alpha_c > \alpha_m$ in more detail: with wave propagation effects difficult to calculate in real materials, $h_i(t)$ and $h_{i+1}(t)$ may be better estimates of each other than $h_i^m(t)$ is of either; with scattering amplitudes difficult to know *a priori* (and difficult to calculate except for families of idealized shapes), $r_i(t)$ and $r_{i+1}(t)$ may be better estimates of each other than $r_i^m(t)$ is of either; therefore, the potential exists for $s_i(t)$ and $s_{i+1}(t)$ to "match" better than $s_i^m(t)$ "matches" either [7-10].

A more complete comparison of the correlation and matched filter approaches reveals the following first order observations: 1) the correlation approach can be implemented without *a priori* calculation of a template, that is, without estimating the signal distortion effects due to scattering at the flaw and without accounting for attenuation, transmission, mode conversion, and diffraction [7-10] – effects that can be argued are inherently contained within adjacent A-scans; 2) the correlation approach has additional noise beyond that of the matched filter; 3) the correlation approach requires the presence of the flaw signal in adjacent A-scans whereas detection for the matched filter approach can be based on a flaw signal in a single A-scan; and 4) when flaw signals are present in adjacent A-scans and the flaw signals are knowable (i.e., $\alpha_m \to 1$), the flaw signals in the adjacent A-scan must also be similar, implying $\alpha_c \to 1$.

Finally, while the measurement position spacing was assumed to be large enough such that adjacent noise signals are uncorrelated, this may not always be the case. Recall that for the correlation approach applied in backscatter, the noise distribution (see Fig. 1(b)) is given by the correlation distribution between adjacent noise signals. Thompson et al. [13]

provide a theoretical framework for the correlation between adjacent noise signals, and Cepel et al. [14] give example correlation coefficient distributions for different measurement position spacings. In fact, the correlation between adjacent backscattered noise signals is influenced by measurement position spacing, by beam field characteristics, and may be influenced by internal material structures (e.g., grain structure) except at long wavelength [2,3,13]. Relative to performance of the correlation approach, with reference to Fig. 1, as the measurement spacing is decreased, the mean of the noise correlation distribution moves to the right [14], resulting in the potential for increased overlap between the noise and signal + noise distributions. This issue is addressed again at the end of the next section.

B. Correlation coefficient calculations

The correlation approach is now developed more formally for a set of measured signals, building on the models introduced above. The correlation of interest is the spatial cross-correlation calculated between gated A-scans measured at adjacent measurement positions. Consider an *N x M* scan with each A-scan *T* points long and using the array $\mathbf{x} = x_{i,j}(t)\ \ i = 1...N\ \ \ j = 1...M\ \ \ t = 0...T-1$ to hold the A-scans. Calculation of the correlation coefficient between A-scans is then given by the following equation where $\hat{\rho} = \hat{\rho}(i, j, \delta_r, \delta_c, \tau)$ is a sample estimate of the associated expected value [1-5]:

$$\hat{\rho} = \frac{\sum_{t=t_i}^{t_f} \left(x_{i,j}(t-\tau) - m_{i,j}\right)\left(x_{i+\delta_c, j+\delta_r}(t) - m_{i+\delta_c, j+\delta_r}\right)}{\sqrt{\sum_{t=t_i}^{t_f} \left(x_{i,j}(t-\tau) - m_{i,j}\right)^2} \sqrt{\sum_{t=t_i}^{t_f} \left(x_{i+\delta_c, j+\delta_r}(t) - m_{i+\delta_c, j+\delta_r}\right)^2}} \tag{4}$$

Normalization removes the scale dependence and restricts $\hat{\rho}$ to the range -1 to 1. In Eq. (4), the summation range in the time-domain defines the portion of the signal (the time window or gate) of interest, m is the mean value calculated over the gate, τ controls the lag or temporal shift between the two signals, and δ is a spatial shift parameter. Throughout the paper, t is used as a discrete index referring to the temporal direction. For clarification, T gives the number of points in each A-scan as digitized and as written into the initial data array; t_i and t_f define the element numbers corresponding to the start and end, respectively, of the time gate or time window for analysis. With $\delta_r = 1,\ \delta_c = 0$, "row correlations" are calculated between adjacent A-scans, that is, A-scans measured at the j^{th} and $j^{th}+1$ positions in the i^{th} scan row. Similarly, with $\delta_r = 0,\ \delta_c = 1$, "column correlations" can be calculated. Correlations for all possible adjacent signal combinations in an N x M raster scan can be calculated using a computation loop over i and j with the spatial shift applied sequentially to i and j.

Before leaving this section, the role of measurement position spacing and the spatial shift parameter, δ, deserve more attention [3,13,14]. The spatial shift parameter can be used to establish an "effective" measurement position spacing or step size that is an integral multiple of the actual step size. For example, if a Cartesian scan is done in 0.1 mm steps, the "effective" step size for correlation of adjacent signals can be increased in 0.1 mm increments by increasing δ_r and δ_c in unit steps. The driving issue here is that the correlation approach requires a balance between reducing the measurement step size and resisting this reduction. Reducing the step size is motivated by the following: a flaw signal must be present in at least a pair of adjacent signals to allow detection – motivating a reduced

step size to increase resolution; as the similarity between adjacent flaw signals increases (i.e., as the similarity between $s_i(t)$ and $s_{i+1}(t)$ increases), the mean of the signal + noise distribution (see Fig. 1(b)) increases, leading to less overlap between the noise and signal + noise distributions – also motivating a reduced step size to improve performance. Conversely, avoiding reduction in the step size is motivated by the following: at some point, as the step size is reduced, the correlation between noise signals increases and the mean of the noise distribution shifts to the right (see Fig. 1(b)), leading to greater overlap between noise and signal + noise distributions – motivating avoidance of a step size reduction in order to improve performance. In terms of achieving this balance, we note that focused probes allow for reducing the step size in order to enhance performance while avoiding the critical step size at which noise correlations will increase and performance will degrade. Beyond this observation, we would say that while parameters which affect performance have been identified, a methodology for optimally selecting these parameters has not yet been established.

C. Signal alignment

Measured signals can be aligned globally and locally. Global signal alignment for backscatter is done by aligning the leading edge of each front surface reflection. Global alignment yields B-scan images aligned at the front surface reflection, providing a basis for evaluating the remaining systematic or random misalignment within the image. This global alignment is only achieved easily and unambiguously under favorable measurement configurations and sample geometries.

Local signal alignment can be used to form locally aligned B-scan images or to form correlation coefficient images based on maximum correlations. In either case, the core

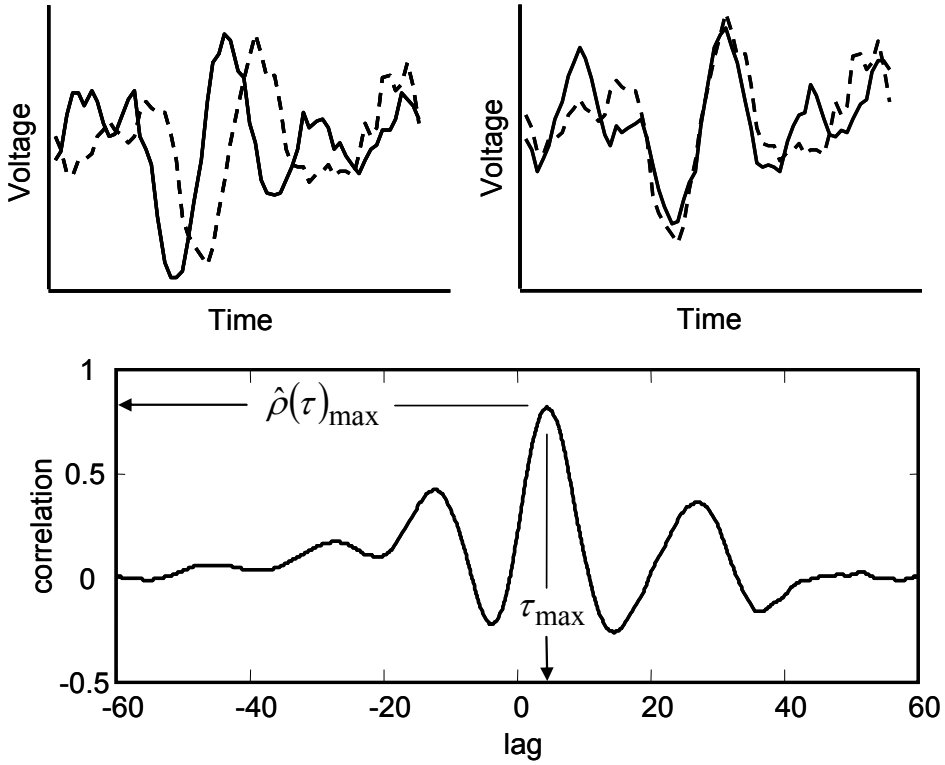

Fig. 2. Example cross-correlelogram along with a pair of signals as-measured and aligned

process involves forming a cross-correlelogram between two signals [1]. The cross-correlelogram is given by a plot of $\hat{\rho}(\tau)$ versus τ. An example of a cross-correlelogram along with a pair of signals as-measured and aligned is shown in Fig. 2. Signals were measured in backscatter from a stainless steel inertial weld sample. From this plot, the maximum correlation, $\hat{\rho}(\tau)_{\max}$, can be extracted along with the shift, $\tau_{\max}$, to the maximum correlation. To perform local signal alignment for B-scan images, each signal is shifted in time by $\tau_{\max}$ for that signal to achieve alignment with a signal chosen as the reference signal. An example of B-scans as-measured and after alignment is shown in Fig. 3, again based on data from the inertial weld sample. To perform local signal alignment to be used in correlation images, $\hat{\rho}(\tau)$ is calculated as given in Eq. (4) between each gated signal and its nearest row and column neighbors. For each pair of signals, $\hat{\rho}(\tau)_{\max}$ is written into a

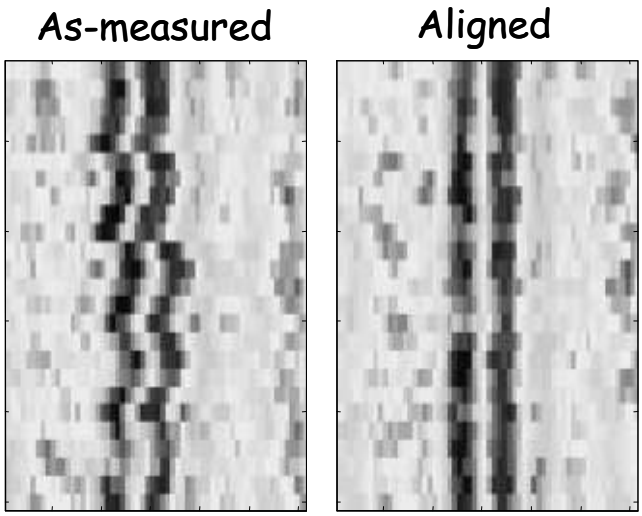

Fig. 3. Example B-scans as-measured and aligned.

new array which is used as a basis for correlation image formation. With the correlation approach, signals are typically allowed to shift over a very limited range under the assumption that adjacent flaw signals will vary in phase by a limited amount. In contrast, in application of matched filtering, the template may be allowed to shift over a wide range in searching for flaw signal. Also note that while local alignment can reveal high correlations in adjacent signals that would have been missed without alignment; the alignment procedure also attempts to align noise signals since the procedure is applied throughout the image. As a result, both the noise and signal + noise distributions shown in Fig. 1(b) generally move to the right, each with reduced variance. The influence of local alignment on detection performance must therefore be considered on a case by case basis.

D. Image display issues

Given A-scans from an N x M scan which have been written into the array $\mathbf{x} = x_{i,j}(t)$, correlation image formation proceeds as follows: establish a time gate, calculate the correlation coefficient between adjacent A-scan in the three-dimensional array, and write these correlations into one or more two-dimensional arrays. Correlations can be calculated

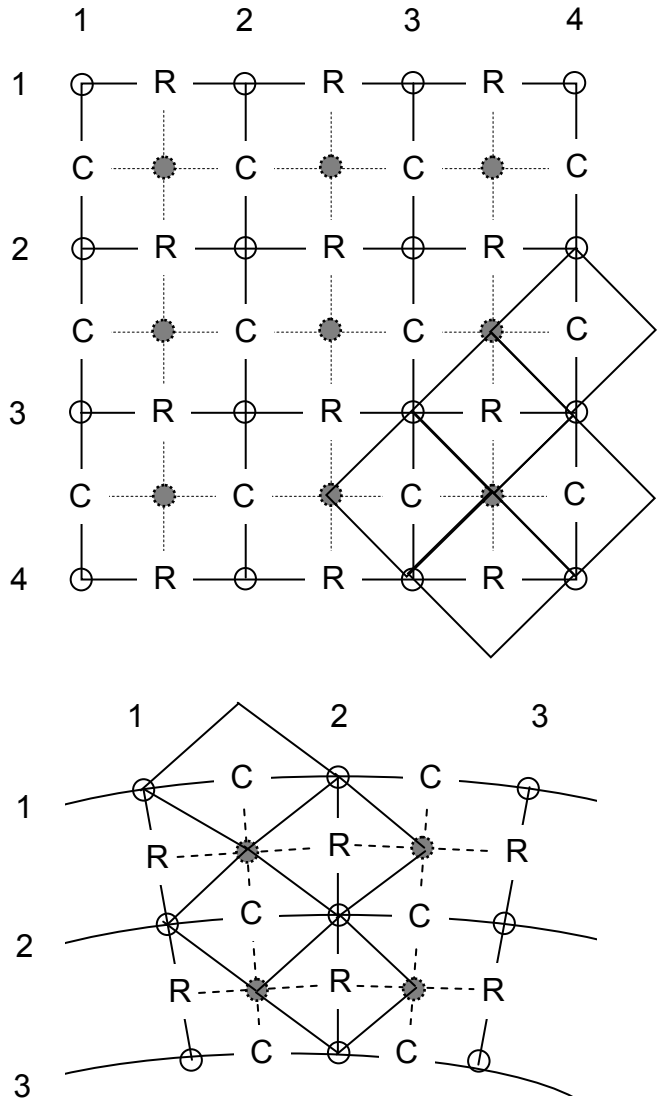

Fig. 4. Schematic representation of Cartesian and polar scans. Open circles represent measurement positions. R's and C's represent the conceptual positions of row and column correlations for a Cartesian scan and radial and circumferential correlations for a polar scan.

with alignment, $\hat{\rho}(\tau)_{\max}$, or without alignment, $\hat{\rho}(0)$. For an N x M scan where correlations are calculated without signal skipping ($\delta_i = 0$), there will be $N(M-1)$ row correlations and $(N-1)M$ column correlations, for a total number of $2NM - M - N$ correlations. Figure 4 shows a schematic representation of a 4 *x* 4 scan (top figure) with open circles at the 16

measurement positions. The R's and C's are used to represent the positions conceptually assigned to the correlation between adjacent row signals and adjacent column signals, respectively. Also shown in the figure is a portion of a polar scan (bottom figure) with the R's and C's now representing the positions assigned to radial and circumferential correlations, respectively, and the open circles again at the measurement positions. At this point, the easiest approach would be to make two correlation images: one based on an *N x (M-1)* row correlation array, given by the equation $imagerow(i,j) = \hat{\rho}\left(x_{i,j}, x_{i,j+1}\right)$, and one based on an *(N-1) x M* column correlation array, given by the equation $imagecol(i,j) = \hat{\rho}\left(x_{i,j}, x_{i+1,j}\right)$. Similarly, radial and circumferential correlation images could be made for a polar scan. This approach is useful in that two images are created which allow separate evaluation of row and column correlations. However, formation of a single correlation image is generally desirable.

The issues associated with forming a single correlation image can be addressed by first thinking in terms of writing the row and column correlations into a single array. In general terms, the $2NM - M - N$ row and column correlations are written into a $(2N-1)\,x\,(2M-1)$ array, leaving $2NM - N - M + 1$ blank elements. For the 4 *x* 4 example (see Fig. 4), the open and filled circles represent the blank element positions in the correlation array. An image could be created based directly on an array containing blank elements, with each blank element assigned the same value; however, the image would be visually unsatisfying with useful correlation values displayed within a regular array of mono-colored pixels.

A variety of solutions exist to this image display problem. One potential solution would be to assign each blank element an average of nearest neighbor values. The resultant

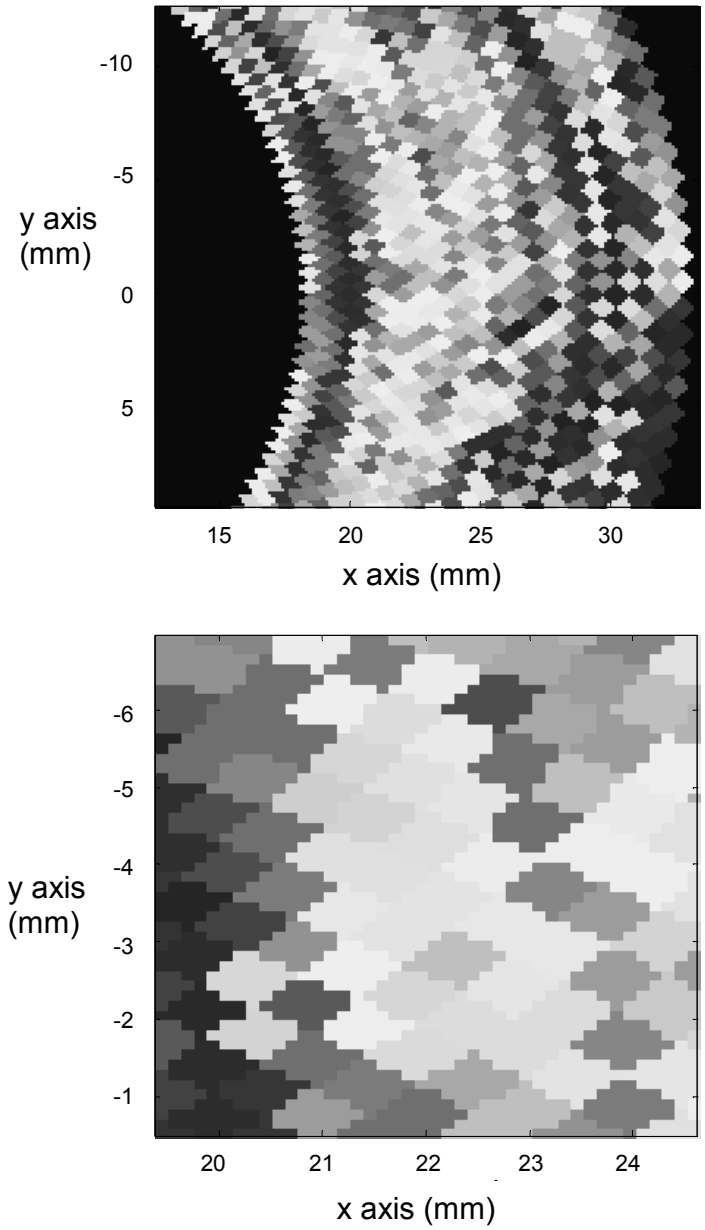

Fig. 5. Example correlation images using the diamond region approach for a polar scan. Each diamond region represents either a radial or circumferential correlation coefficient. Images are shown at high magnification in order to reveal pixelization details.

image would be composed of pixels associated with row correlations and column correlations and pixels which are an average of row and column correlations. A second approach is to shift the column correlations up one row, with the resulting image formation equations being

$image(i,2j-1)=\hat{\rho}(x_{i,j},x_{i+1,j})$ and $image(i,2j)=\hat{\rho}(x_{i,j},x_{i,j+1})$. This approach compromises spatial registration somewhat; however, the resultant images are useful for qualitative evaluation. A third approach which preserves spatial registration is to consider each correlation value as being centered in a diamond-shape region (see Fig. 4). To facilitate display, the diamond regions are discretized using a large number of Cartesian elements with each element assigned a value based on which diamond that element falls within. As shown in the blown-up polar correlation image in Fig. 5, a close look at a correlation image reveals the diamond shaped regions and the discretization.

IV. Results

Two example results are show which cover polar and Cartesian scans and detection based on decreased and increased correlation, respectively. In each case, companion C-scan images are shown for comparison purposes.

Figure 6 shows a C-scan image (top) and correlation image (bottom) for the stainless steel annular ring. Data were measured in a polar scan with the correlation image displayed using the diamond region format. Starting from the top and moving clockwise, there are three 1/16", one 2/16", and one 3/16" diameter flat-bottom-holes. In both images, the five flat-bottom-holes are clearly visible; however, for the smaller holes the contrast between the flat-bottom-hole region and the background noise is greater in the correlation image than in the C-scan image. Note that the background noise in the correlation image is associated with correlation coefficients for grain noise signals. Detection of the flat-bottom-holes is possible due to relatively high correlations between signals containing echo signals from a given flat-bottom-hole; that is, correlations that are high relative to correlations associated with grain noise signals. In general, as depicted in Fig. 1(b), there will be an overlap between the noise

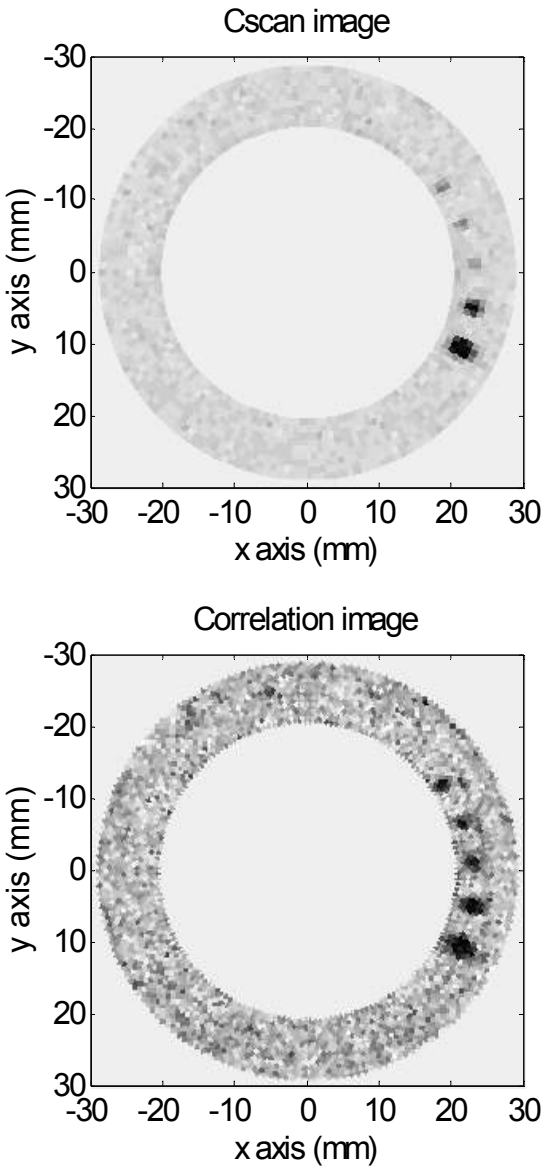

Fig. 6. Example correlation image (bottom) and C-scan image (top) showing 5 flat bottom holes in a stainless steel annular ring. The correlation image was formed using the diamond region approach. The darker regions in the images represent high correlations and high amplitudes, respectively.

and signal + noise distributions. As such, there is a chance for false-calls, and the choice of a detection threshold must strike a balance between false-calls and missed-defects. In this particular example, even though there are additional regions around the annular image that appear rather dark on the grey-scale image, the correlations associated with each flat-bottom-

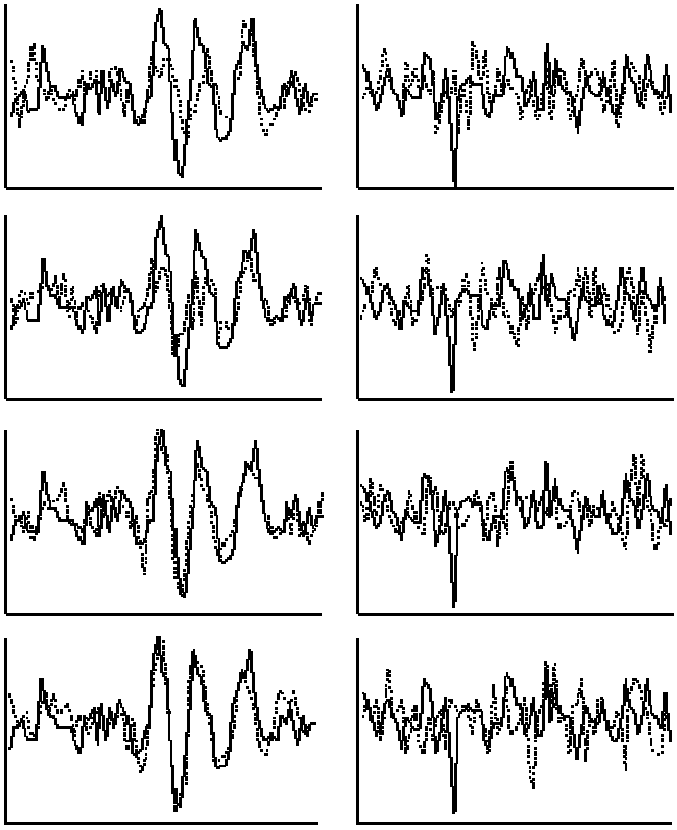

Fig. 7. Example A-scans from a flat-bottom-hole region (left) and a grain noise region (right). The center signal in a group of 5 signals is shown in solid line. In the correlation approach, this signal is correlated with each of its 4 closest neighboring signals (shown in dashed line). By observation, the correlation between adjacent signals measured from the flat-bottom-hole region is significantly higher than the correlations between adjacent grain noise signals.

hole are substantially higher than any of the other groupings of correlations around the image. Finally, note that image processing routines can be applied to each image to provide some degree of enhancement.

As a concrete example of the increased similarity between flat-bottom-hole echo signals relative to the similarity in grain noise signals, Fig. 7 shows A-scans from a flat-bottom-hole region and from a grain noise region. In this example, two groups of 5 gated A-

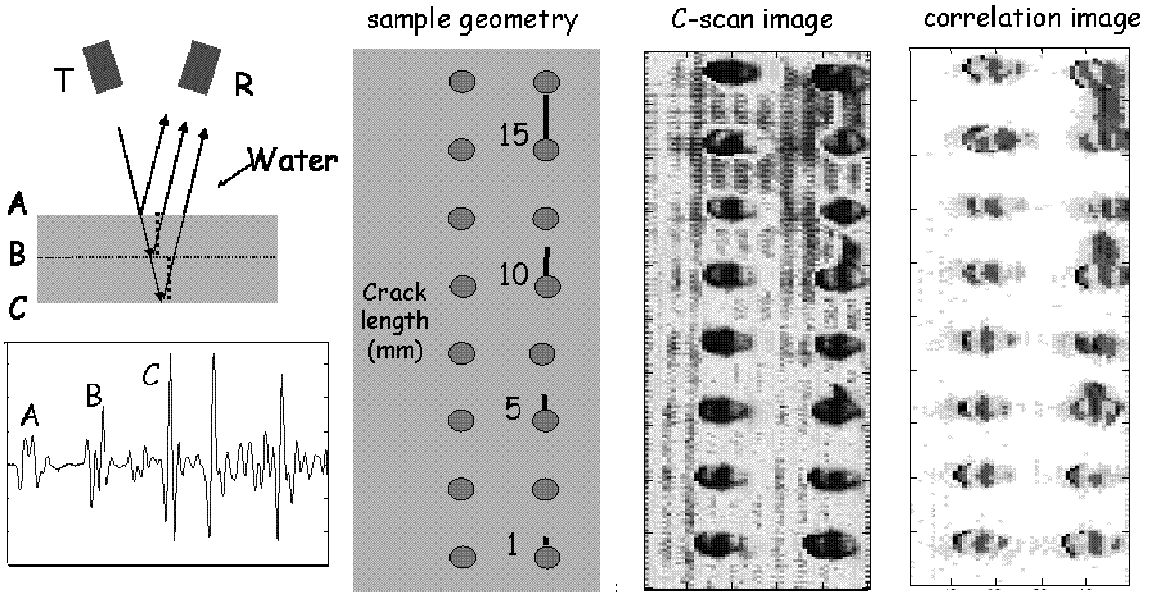

Fig. 8. Example of crack detection in pitch-catch based on decreased correlations. Darker regions in the C-scan image represent decreased amplitude. Darker regions in the correlation image (formed using the interleaving approach) represent decreased correlations.

scans are shown. In each case, the center signal in the group of 5 is shown in solid line along with its 2 neighboring signals radially and its 2 neighboring signals circumferentially (all shown in dashed line). The basis for correlation image formation is the correlation neighbors. Figure 7 provides visual insight into the contrast in correlation between signals from a flat-bottom-hole region and signals from a grain noise region. In this example, the signals from the flat-bottom-hole region (left column) clearly show a higher correlation than the signals from the grain noise region (right column).

The second example is based on measured oblique incidence pitch-catch data from the aluminum sample. The schematics in Fig. 8 show the sample geometry. The sample is made up of two aluminum plates joined together with two rows of eight fasteners with sealant between the two plates. EDM notches were machined to extend from four of the fastener holes in the outer aluminum plate (the skin) at four different lengths as shown in the

figure. Images are based on the interface reflection (signal B) at the faying layer. Similar results are obtained by monitoring signal C from the back surface of the substructure. In this case, interaction of the acoustic beam with the EDM notches causes amplitude reduction and distortion of the transmitted signal. The reduction in amplitude makes the presence of the notches apparent in the C-scan image. The distortion leads to a reduction in signal correlation, making the notches detectable in the correlation image. The three longer notches are easily detected and sized in either image with the 1 mm notch difficult to detect without ambiguity. The vertical striping, especially prominent in the C-scan image, is likely associated with aluminum fabrications processes. Again, image processing techniques can be applied to enhance either image.

V. Summary and discussion

The correlation approach outlined in this paper is attractive as a potential compliment to the classical C-scan approach for a number of reasons including: the correlation approach is scale independent; the correlation approach relies on signal shape, while the C-scan approach uses only the peak value; correlations are calculated based on the same A-scans used in forming C-scan images; correlation images have a qualitatively similar appearance to C-scan images, facilitating inspector acceptance; and correlation images can be formed without the expertise required to deal explicitly with wave propagation and scattering effects.

In terms of additional development on the correlation approach, work is underway in two areas. First, a formal ROC analysis, which is in progress, should shed light on the performance of the correlation approach in comparison to the C-scan and matched filtering approaches [4]. As part of this analysis, data fusion is being used to assess performance of the correlation, C-scan, and matched filtering approaches combined. We note, however, that

any simulation or model based performance comparison will be heavily influenced by underlying assumptions related to signal distortion. Specifically, with reference to the model development section, relative performance will be substantially controlled by the amount of scattering based distortion allowed, through $r_i(t)$; by the extent to which $r_i^m(t)$ is allowed to "match" $r_i(t)$; and by the extent to which $r_i(t)$ and $r_{i+1}(t)$ are allowed to "match." And finally, the correlation approach is amplitude independent but is not measurement system or material independent. Preliminary assessment has shown very weak dependence of correlation values on the beam field near the focal region of a focused transducer. Future work will include a more in depth study of the influence of beam field variations, frequency content, and material morphology on the correlation approach.

Acknowledgements

This work was supported by the Center for Aerospace Manufacturing Technology (CAMT) at the University of Missouri-Rolla (UMR) funded under Air Force Research Laboratory Contract FA8650-04-C-5704 and by Boeing under PO Z40791. Previous support for development of the correlation approach was provided by Honeywell Federal Manufacturing and Technology and by the National Science Foundation (NSF CMS 9610189). The authors would like to acknowledge contributions to this work at various stages by Dr. Mark D. Russell (while a postdoc at the University of Missouri-Columbia (MU)) and Dr. Lori Thombs (Department of Statistics at MU) along with Eric Jamieson, Jose A. Samayoa, and Jason P. Miller from Honeywell FM&T. In particular, the encouragement by Eric Jamieson to extend the correlation approach to more localized flaw detection was pivotal. Many thanks are also due to Dr. Zoughi from UMR for his administrative role in CAMT.

References

1. J. S. Bendat and A. G. Piersol, *Engineering Applications of Correlation and Spectral Analysis*, J. Wiley, New York, p. 46, 1993.

2. W. F. Walker, "The significance of correlation in ultrasound signal processing", *Proc. SPIE Vol. 4325, Medical Imaging: Ultrasonic Imaging and Signal Processing*, edited by Michael F. Insana and K. Kirk Shung, 2001, pp. 159-171.

3. B. A. Rinker, E. E. Jamieson, J. A. Samayoa, T. G. Abeln, T. P. Lerch, and S. P. Neal, "Detection of weak interface signals for same material bond/weld inspection", *Review of Progress in Quantitative Nondestructive Evaluation*, Vol. 22B, edited by D. E. Chimenti and D. O. Thompson, AIP, Melville, 2003, pp. 1080-1087.

4. R. Cepel, K. C. Ho, B. A. Rinker, D. D. Palmer, Jr., and S. P. Neal, "Ultrasonic detection using correlation images", *Review of Progress in Quantitative Nondestructive Evaluation*, Vol. 26, edited by D. E. Chimenti and D. O. Thompson, AIP, Melville, 2007, (in press).

5. S. M. Kay, Fundamentals of Statistical Signal Processing Volume II Detection Theory. Prentice-Hall, Upper Saddle River, NJ, 1998.

6. A. D. Whalen, Detection of Signals in Noise, New York: Academic Press, 1971.

7. J. Q. Xin, K. D. Donohue, and N. M. Bilgutay, "Filter design for ultrasonic flaw echo detection in large-grained material", *Review of Progress in Quantitative Nondestructive Evaluation*, Vol. 10A, edited by D. E. Chimenti and D. O. Thompson, Plenum Press, New York, 1991, pp. 725-731.

8. C. P. Chiou, R. B. Thompson, and L. W. Schmerr, "Model-based signal processing techniques for ultrasonic flaw detection: simulation studies", *Review of Progress in Quantitative Nondestructive Evaluation*, Vol. 12A, edited by D. E. Chimenti and D. O. Thompson, Plenum Press, New York, 1993, pp. 703-710.

9. K. Srinivasan, C. Chiou, and R. B. Thompson, "Ultrasonic flaw detection using signal matching techniques", *Review of Progress in Quantitative Nondestructive Evaluation*, Vol. 14A, edited by D. E. Chimenti and D. O. Thompson, Plenum Press, New York, 1993, pp. 711-718.

10. H. Eriksson, P. O. Borjesson, P. Odling, and N. G. Holmer, "A robust correlation receiver for distance estimation", *IEEE Trans. Ultrason. Ferroelectr. Freq. Control*, **41**(5), 506-603, (1994).

11. V. Murino and A. Trucco, "A confidence-based approach to enhancing underwater acoustic image formation", *IEEE Trans. Image Processing*, **8**(2), 270-285, (1999).

12. J. M. Seixas, F. P. Freeland, and W. Soares-Filho, "Matched filters for identifying failed fuel rods in nuclear reactors", Electronics, Circuits and Systems, 2001, ICECS 2001, The 8th IEEE International Conference on, 2, 643-646, (2001).

13. R. B. Thompson, L. Yu, and F. J. Margetan, "A formal theory for the spatial correlation of backscattered ultrasonic grain noise", *Review of Progress in Quantitative Nondestructive Evaluation*, Vol. 24, edited by D. E. Chimenti and D. O. Thompson, AIP, Melville, 2005, pp. 1292-1299.

14. R. Cepel, L. Thombs, K. C. Ho, and S. P. Neal, " Statistical analysis and computer generation of spatially correlated acoustic noise", *J. Nondestr. Eval*., (in press).

15. A. Dogandzic and N. Eua-Anant, "Defect detection in correlated noise", *Review of Progress in Quantitative Nondestructive Evaluation*, Vol. 23A, edited by D. E. Chimenti and D. O. Thompson, AIP, Melville, 2004, pp. 628-635.

CHAPTER 3
STATISTICAL ANALYSIS AND COMPUTER GENERATION OF SPATIALLY CORRELATED ACOUSTIC NOISE

by

Raina Cepel, Lori Thombs, Dominic Ho, and Steven P. Neal

Abstract:

In ultrasonic NDE, simulation studies can play an important role in complimenting experimental validation of techniques under development. The utility of such simulations depends, in part, on the degree to which the simulated defect and noise signals are representative of the measured signals. In this paper, we describe an approach for generating simulated acoustic noise with a spatial correlation coefficient distribution and maximum extreme value (MEV) distribution which matches those distributions for measured acoustic noise. The procedure for generating noise signals is outlined for a line scan and for a raster scan. The basic approach forces the correlation of neighboring signals to the desired correlation by creating each signal as the sum of appropriately scaled neighboring signals plus a new random signal. For the line scan where each interior position has only two neighbors, this process is done sequentially without iteration. For the raster scan where each interior point has four nearest neighbors, iteration is required to simultaneously achieve the desired correlations with row and column neighbors. The MEV distribution is controlled in an outer iterative loop with the shape and position of the distribution dictated by spectral content of the noise signals and by controlling the signal energy, respectively. Results are shown which demonstrate the effectiveness of the approach. With this approach, a limited number of measured signals can be used to establish the correlation coefficient and MEV distributions which drive the computer generation of a large number of simulated acoustic noise signals.

I. Introduction

Simulation studies are routinely used in ultrasonic nondestructive evaluation (NDE) to complement experimental studies during the development of new inspection approaches. Simulated A-scans typically include a target signal (e.g., a flaw or weld plane signal) plus noise. The noise of interest lies between the front and back surface reflections in an A-scan and is comprised of electronic plus acoustic noise. In certain cases, the degree of correlation between A-scans can have a significant influence on detection.[1-4] These correlations can be quantified in terms of the spatial cross-correlation, at zero lag, between gated A-scans.[4,5] Uncorrelated noise A-scans are easily generated using a normal random number generator with filtering used to achieve the desired frequency content. Margetan et al. have gone a step further using an independent scatterer model to generate simulated grain noise A-scans with correlations between A-scans controlled to some degree through use of an experimentally determined spatial correlation length parameter.[2] Using their approach, the average, maximum, and standard deviation of gated peak-values are also controlled. In the current paper, we describe an approach for generating simulated acoustic noise with a correlation coefficient distribution and maximum extreme value (MEV) distribution (i.e, the gated peak-value distribution) which matches those distributions determined for measured acoustic noise.

The motivation for this project finds its origin in research associated with kissing bond detection for inertial welding of two stainless steel pieces. Kissing bonds can be very difficult and expensive to fabricate in a controlled fashion, providing motivation for simulation studies which utilize simulated noise signals with realistic correlation coefficient distributions. The basic approach being developed relies on the correlation coefficients

between adjacent A-scans to detect low signal-to-noise ratio (SNR) kissing bond signals. This approach finds its genesis in the work of Nagy and Adler on this same problem.[6] Without going into the analysis details, suffice it to say that an inspection approach can be formulated which relies heavily on the comparison between correlation coefficient distributions associated with backscattered signals from the weld being inspected and from a known set of acceptable welds.[7] More recently the correlation approach has been extended to crack detection in both pulse/echo and pitch/catch.[8]

Computer generation of correlated random variables with a desired mean correlation coefficient is straightforward. For example, the i^{th} random sample can be generated based on the $i^{th} - 1$ random sample as follows: [5]

$$x(i) = a(i) + bx(i-1) \tag{1}$$

where b is an adjustable scale factor, $a(i)$ is the output of a random number generator, and the x's are the computer generated samples of the random variable, **x**. The single scale factor can be adjusted to yield the desired mean correlation coefficient value, but, in general, the scale factor cannot be adjusted such that desired correlation coefficient mean and distribution (width and shape) are achieved. The natural relationship between the mean and shape dictate that as b is increased, correlation values are forced closer to the limiting value of 1.0, the distribution breadth decreases, and the distribution becomes increasingly skewed with a fat lower tail. The primary task addressed in this paper is to extend the approach represented in Eq. (1) so that vectors of random numbers (simulated A-scans) can be generated that show

the desired distribution of correlation coefficient values. These simulated signals will also be forced to the desired MEV distribution.

Simulation of data with specified correlation structure arises in many fields. In the physical sciences, scientists often use Shewhart Control Charts to monitor a process. In this setting, data are a time-indexed series of averages or counts taken at regularly spaced time intervals. Padgett, Thombs and Padgett [9] present a method to generate such one-dimensional data with specified mean and variance structure so that the performance of such charts can be studied via simulation. In this paper, the generated data are two dimensional, with emphasis on both the correlation within and between series, as well and the maximum extreme value distribution.

Two dimensional spatial time series data with correlation structure is common in many other areas, including meteorology, hydrology and ecological and environmental studies. In the area of ecology and wildlife studies, observations such as animal counts are typically observed at irregularly-spaced locations. Neighboring observations are likely to be correlated, and the paper by Brooker [10] represents one of the first attempts to generate such data.

In spatial statistics, point patterns are observed on variables such as temperature and rainfall, so that the data often include a (third) component, time. See Cressie [11] for more information on the statistical aspects of fitting models to such data. A recent contribution by Kyriakidis et al.[12] proposes an algorithm for generating spatio-temporal precipitation data, with emphasis on preserving the distribution of the original data set. Data are both space-indexed (e.g., longitude and latitude) and time indexed.

The methodology presented in the current paper is distinct from these related approaches for generating dependent data in that both the correlation and the MEV distribution are controlled. The paper proceeds by first establishing representative correlation coefficient and MEV distributions associated with measured backscattered noise. The methodology for generation of simulated acoustic noise with the desired correlation coefficient and MEV distributions is then described for a line scan and for a raster scan. Results are presented which validate the approach for the experimentally established correlation coefficient and MEV distributions. The paper closes with a brief summary section.

II. Measurement Procedure

Backscattered grain noise signals were measured and used as a basis for calculating associated correlation coefficient and MEV distributions. The ultrasonic measurement system used in these measurements consists of a water tank filled with degassed tap water at approximately 19^{o}C, a three dimensional scanning bridge that holds a transducer, a pulser-receiver unit, and a 12 bit data acquisition card with a sample rate of 100 MS/s. A dedicated PC collects data from the acquisition card and controls the motor controller that moves the scanning bridge. A separate PC is employed for data analysis.

The transducer used to make measurements was a focused ½" transducer with a 10 MHz center frequency and a 4" focal length. The settings on the pulser-receiver and the data acquisition card were typically set at values such that the front and back surface reflections were blown off the screen in order to enable proper digitization of the grain noise. In each measurement position, 64 signals were taken and averaged together in order to reduce electronic noise.

The sample used in all measurements was a stainless steel plate with the dimensions 10.1 x 5 x 1.9 cm. A leveling plate was used to ensure that the specimen was aligned with the transducer's scan plane. The transducer was normalized in relation to the front face of the sample. Data was taken at a single water path such that the focal point of the transducer would be approximately at the sample mid-plane. Signals were measured on a 3.2 x 2.4 cm grid with 0.5 mm between measurement positions.

After the data was collected, pre-processing was done on the raw signals. First, the front surface reflections of each signal were aligned with one another. Then all of the signals were averaged together in order to identify any non-random component associated with the front surface reflections. This mean signal was subtracted from each of the individual signals so that spatial correlations between adjacent noise signals could be calculated with minimal influence from front surface reflection ringing.[2] Finally, each signal was gated to extract a time window of 51 points (0.50 μs) with the gate positioned to correspond closely with the location in the sample where the transducer was focused.

III. Statistical Analysis of Measured Noise

A. Maximum Extreme Value Distributions

Vectors of data representing maximum extreme values (maximum absolute values) for the measured noise were extracted from the gated signals. Figure 1 shows 2 histograms based on this MEV data. The lower histogram is for all measured signals, that is, for a measurement position spacing of 0.5 mm. The upper histogram is for every 3rd signal, corresponding to a measurement spacing of 1.5 mm. The histograms are fundamentally the same with the number of observations being the only significant difference. An extreme

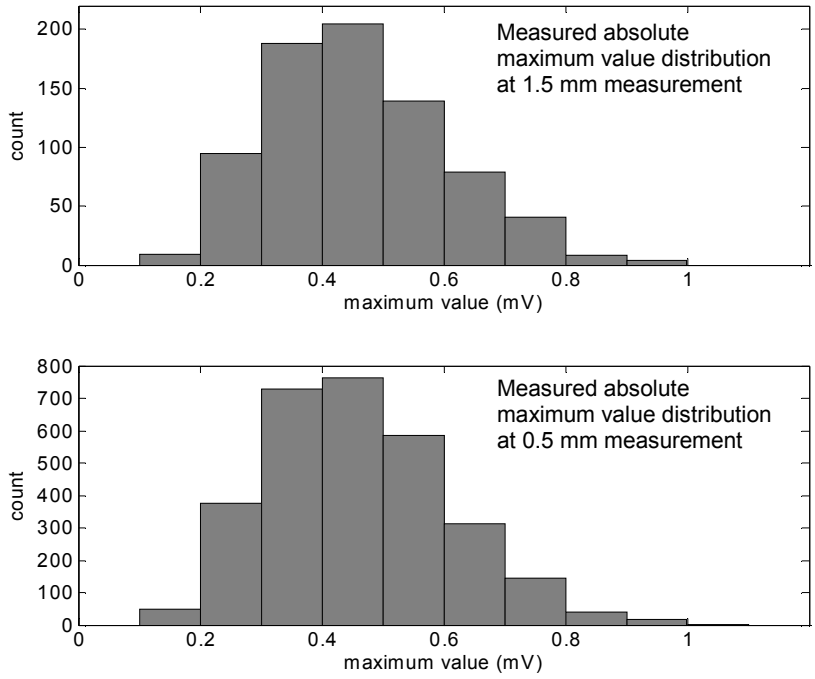

Fig. 1. Histograms of maximum extreme values for 1.5 mm (upper) and 0.5 mm (lower) measurement position spacing.

value distribution based on the absolute value of the difference between min and max values could have been utilized instead.[2]

B. Spatial Correlation Coefficient Distributions

The correlation of interest is the spatial cross-correlation calculated at zero lag between gated A-scans measured at adjacent measurement positions. For discussion purposes, consider an *N x M* scan with the A-scan (each *T* points long) written into the matrix $\mathbf{x} = x(i,j,t)\; i = 1,N\;\; j = 1,M\;\; t = 0,T-1$ (see Fig. 2). Calculation of the correlation coefficient between A-scans is then given by the following equation where $\rho = \rho(i,j,t_i,t_f,\delta_r,\delta_c)$:

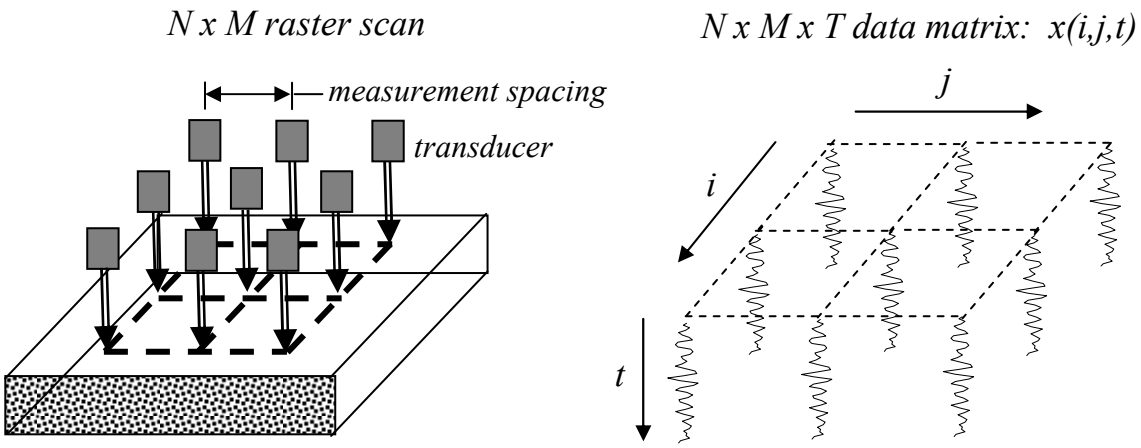

Fig. 2. Representation of measurement positions and associated data matrix.

$$\rho = \frac{\sum_{t=t_i}^{t_f}\left[x(i,j,t)-m_x(i,j)\right]\left[x(i+\delta_c,j+\delta_r,t)-m_x(i+\delta_c,j+\delta_r)\right]}{\sqrt{\sum_{t=t_i}^{t_f}\left[x(i,j,t)-m_x(i,j)\right]^2}\sqrt{\sum_{t=t_i}^{t_f}\left[x(i+\delta_c,j+\delta_r,t)-m_x(i+\delta_c,j+\delta_r)\right]^2}} \quad (2)$$

In Eq. (2), the summation range in the time-domain defines the portion of the signal (the time window or gate) of interest, m is the mean value calculated over the gate, and δ is a spatial shift parameter. Throughout the paper, t is used as a discrete index referring to the temporal direction. With $\delta_r = 1$ $\delta_c = 0$, row correlations are calculated between adjacent A-scan, that is, A-scans measured at the j^{th} and $j^{th}+1$ positions in the i^{th} scan row. Similarly, with $\delta_r = 0$ $\delta_c = 1$, column correlations can be calculated. Correlations for all possible adjacent signal combinations in an *N x M* raster scan can be established using a computation loop over *i* and *j* with the spatial shift applied sequentially to *i* and *j*.

In order to define desired distributions of spatial correlation coefficients for simulated noise, conditional correlation coefficient distributions were established based on the pre-processed measured noise signals. In this section, we begin by considering the overall

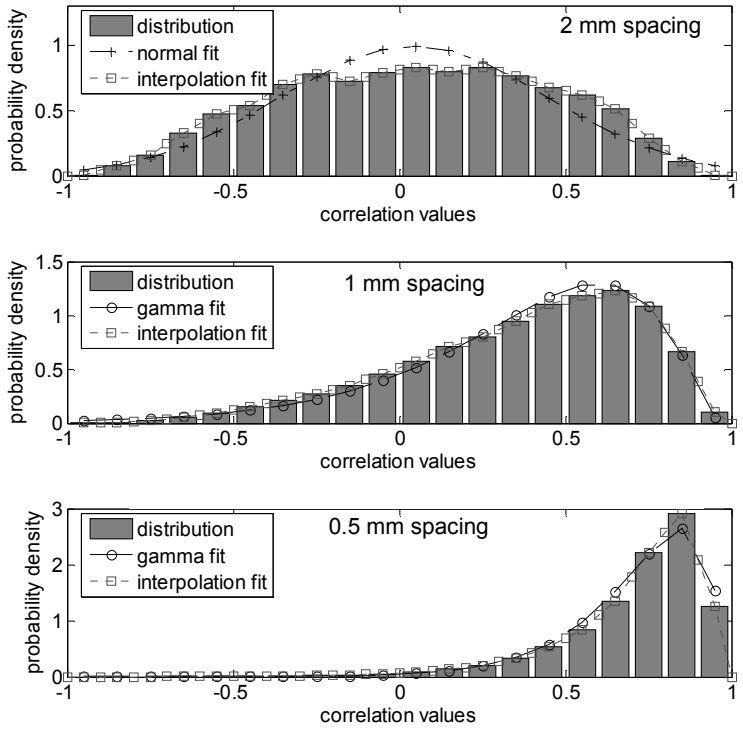

Fig. 3. Histograms of spatial correlation coefficients and associated fits for 2 mm (upper), 1 mm (middle), and 0.5 mm (lower) measurement position spacing.

distribution of correlation coefficients. Conditional distributions are addressed below. The first step was to calculate the correlation coefficient (Eq. 2) between each signal and its row and column neighbors (see Fig. 2) and write these values into a single vector. This calculation was done separately for three measurement spacings: 0.5 mm spacing (every signal), 1 mm spacing (every 2nd signal), and 2 mm spacing (every 4^{th} signal). The correlation coefficient histograms for these measurement spacings are shown in Fig. 3. The influence of measurement spacing on both the mean and the shape of the correlation coefficient distribution is apparent. Conditional correlation coefficient distributions show the same basic characteristics as these overall distributions.

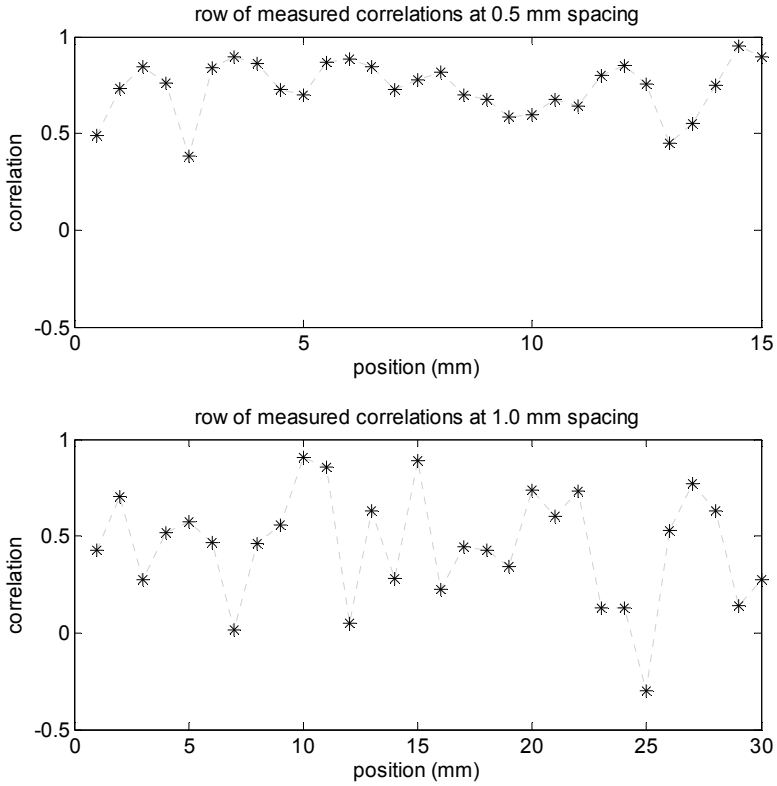

Fig. 4. Variations in spatial correlation coefficients along a line scan for 0.5 mm (upper) and 1 mm (lower) measurement position spacing.

Probability density function fits to the distributions were considered. The normal and gamma distributions were found to be the two common distributions that yielded the best fit to the correlation distributions. The normal distribution works best when the average correlation value is near zero and the distribution is symmetric; however, as is apparent from the figure, the distribution tends to show a suppressed peak and fatter tails than the normal distribution. The gamma distribution works well for skewed distributions with higher average correlations. In some cases, a standard distribution which shows reasonable fit to the histogram cannot be found; however, an interpolation of the histogram can be used to approximate the actual distribution of the correlation coefficient values. The interpolation approach utilizes the Matlab routine randsample to randomly choose a bin and then randomly select a value from each bin based on a linear probability density function defined between the edges of each bin.[13] Superimposed on each histogram in Figure 3 is a normal or gamma distribution fit along with the interpolation fit.

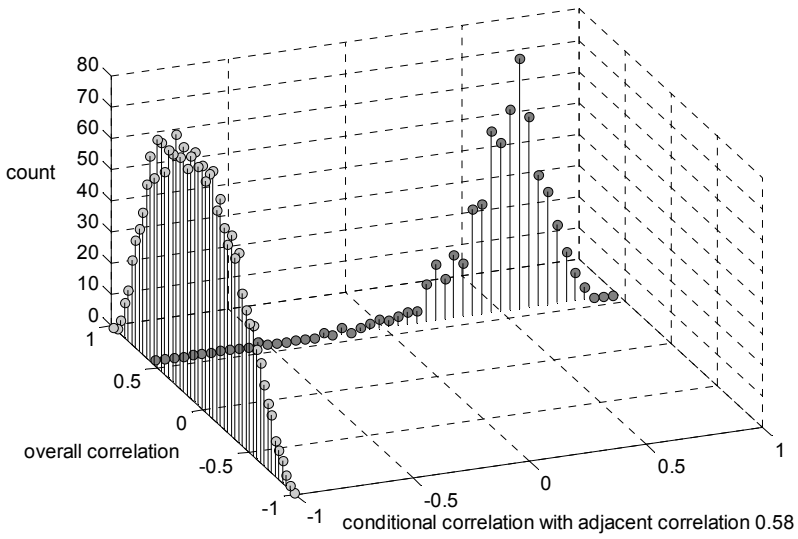

Fig. 5. Stem plots of overall and conditional correlation coefficient distributions. The conditional distribution is for an adjacent correlation coefficient of 0.58.

In general, correlation coefficient values are not randomly distributed in space. That is, the correlation coefficient between a given pair of signals depends on the correlation coefficients between surrounding pairs of signals. As an example, Fig. 4 shows the variation in correlation values along a line scan with relatively low (upper graph) and high (lower graph) measurement spacing. As demonstrated in the figure, the dependence of correlation values on adjacent values decreases with increasing measurement spacing. A graphical example of a conditional histogram is shown by the stem-plot in Fig. 5. The overall distribution is given by stems terminating in light circles, and the conditional distribution, assuming an adjacent correlation value of 0.58, is given by the stems terminating in dark circles.

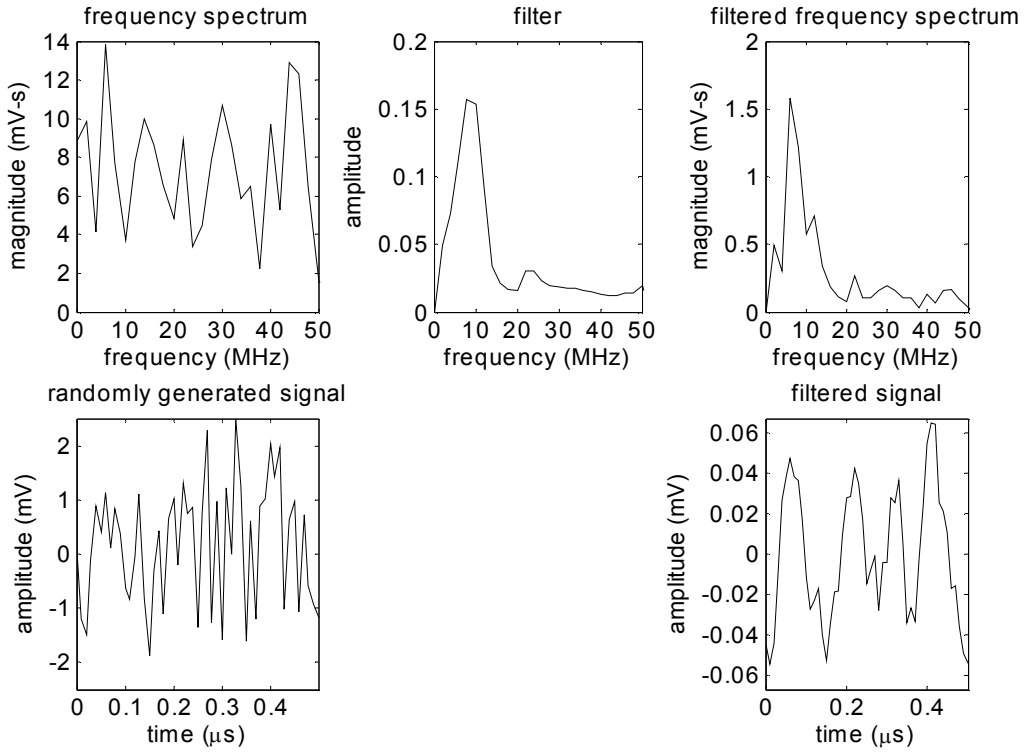

Fig. 6. Steps used in creating spatially uncorrelated acoustic noise with the desired frequency content: (a) white noise signal generated using a standard normal random number generator; (b) spectrum of white noise signal; (c) filter determined based on the average magnitude spectrum of the measured acoustic noise signals; (d) spectrum after filtering; and (e) inverse Fourier transform of filtered spectrum.

IV. Generation of Spatially Correlated Noise

A. Generation of Spatially Uncorrelated Acoustic Noise

A number of equally effective approaches could be taken to generate uncorrelated acoustic noise. As depicted in Fig. 6, the basic steps in the process as implemented here are as follows: 1) using a standard normal random number generator, create a time-domain white noise signal, T points long, for each (simulated) measurement position; 2) Fourier transform each signal to the frequency domain; 3) filter each signal using a filter (with unit energy) that will force the resultant noise to have the same average power spectrum as the measured noise; and 4) inverse Fourier transform each signal back to the time-domain to

yield A-scans which are spatially uncorrelated with appropriate frequency content. Note that the correlated noise creation step described below involves sums of scaled A-scans. This process changes the average power spectrum from the desired spectrum associated with these initial spatially uncorrelated signals. An iterative correction approach will be outlined which brings the average power spectrum back to the desired shape while still achieving the desired correlation distribution was implemented.

B. One Dimensional Generation of Spatially Correlated Noise

We begin by establishing the approach for a line scan and then expand the procedure for application to an *xy* raster scan in the next section. Starting at the noise measurement stage, assume that a line scan is performed, acoustic noise signals are measured and pre-processed, the average power spectrum is estimated, and the overall and conditional correlation coefficient distributions are established. The line scan of measured signals are written in a two-dimensional matrix, denoted $\mathbf{x}_m$, with average power spectral density function estimate and associated magnitude spectrum given by $|\mathbf{X}_m(f)|^2$ and $|\mathbf{X}_m(f)|$, respectively.

For discussion purposes, assume that an N position line scan is to be simulated. $N-1$ correlation coefficients are randomly generated with the first value coming from the overall distribution and subsequent values drawn from conditional correlation coefficient distributions. These $N-1$ correlation coefficients, denoted $\tilde{\rho}(i)\ i=2,N$, will dictate the correlations between simulated noise signals.

Clarification of the overall and conditional correlation coefficient distributions is in order. The overall distribution is the probability density function associated with the probability $P(\rho(i))$, that is, for the entire set of correlation coefficients given that these

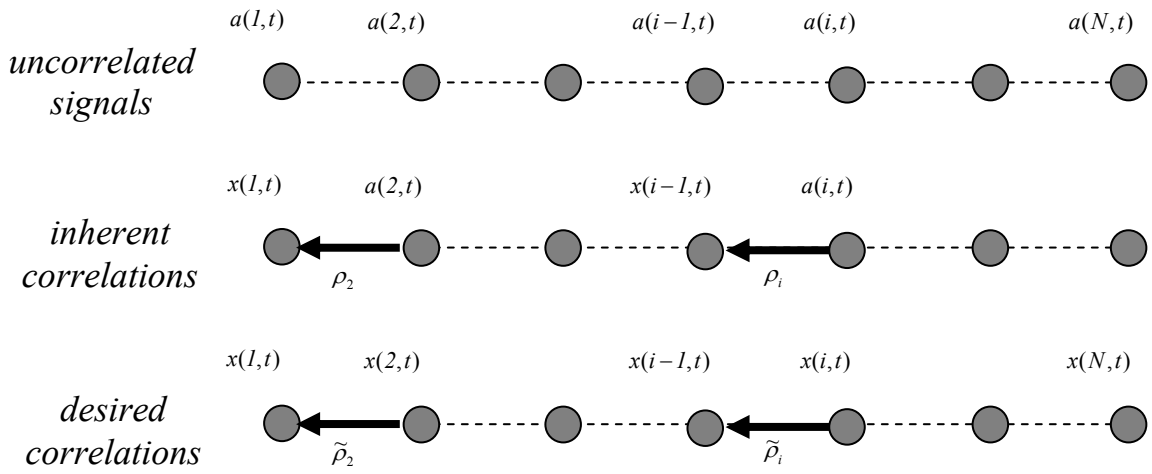

Fig. 7. Representation of the notation and steps involved in creating a simulated line scan of spatially correlated signals.

correlation coefficients are not independent. Before addressing conditional distributions, recall the notation: $\rho(i)$ gives the correlation between $x(i,t)$ and $x(i-1,t)$; $\rho(i-1)$ gives the correlation between $x(i-1,t)$ and $x(i-2,t)$; and $\rho(i+1)$ gives the correlation between $x(i+1,t)$ and $x(i,t)$. Considering only nearest neighbors, the conditional probability density function for $\rho(i)$ is associated with the probability: $P(\rho(i)|\,\rho(i-1)\text{ and }\rho(i+1))$. In practice, during the sequential generation of correlated signals, the correlation coefficient $\rho(i)$ is drawn from the distribution associated with $P(\rho(i)|\,\rho(i-1))$ since $\rho(i+1)$ does not yet exist.

The process of creating correlated noise signals involves several steps. We begin by describing the procedure used to force the desired correlation between to two given signals. This approach is then incorporated into an iterative procedure used to simultaneously match the desired correlation distribution and average power spectrum.

Figure 7 gives a cartoon representation of the notation and some of the steps involved in creating a simulated line scan of spatially correlated signals. Using the procedure

described in the previous section, the first step is to create a set of N uncorrelated acoustic noise signals, represented by the matrix $\mathbf{a} = a(i,t)\ \ i = 1, N\ \ t = 0, T-1$. The output matrix, i.e., the set of correlated signals, is denoted $\mathbf{x} = x(i,t)\ \ i = 1, N\ \ t = 0, T-1$. The next step is to set $x(1,t)$ equal to $a(1,t)$, that is, $x(1,t) = a(1,t)\ \ t = 0, T-1$. Throughout the remainder of the paper, all operations will be implicitly carried out over the range of t, for example, $x(1,t) = a(1,t) \Rightarrow x(1,t) = a(1,t)\ \ t = 0, T-1$. The second signal, $x(2,t)$, is then to be determined so that the correlation between $x(2,t)$ and $x(1,t)$ is equal to the desired correlation, $\tilde{\rho}(2)$. Consistent with approach of Eq. (1), the method used to calculate $x(2,t)$ is to add $b(2)x(1,t)$ to the uncorrelated signal $a(2,t)$: $x(2,t) = a(1,t) + b(2)x(1,t)$. The key is to find the value of $b(2)$ which forces the correlation between $x(1,t)$ and $x(2,t)$ to be equal to $\tilde{\rho}(2)$. This process will be repeated for each signal, that is:

$$x(i,t) = a(i,t) + b(i)x(i-1,t) \qquad i = 2, N \tag{3}$$

Note that $x(i,t)$ will be appropriately correlated with both of its neighbors, $x(i-1,t)$ and $x(i+1,t)$, since the process forces correlations between $x(i,t)$ and $x(i-1,t)$ and between $x(i+1,t)$ and $x(i,t)$.

The process for establishing the scale factor, $b(i)$, can be described as follows. We begin by using the correlation coefficient between $a(i,t)$ and $x(i-1,t)$ to calculate the inherent similarity between the two signals that will be used to create the output signal.

$$\rho(i) = \frac{\sum_{t=0}^{T-1} \left(a(i,t) - m_a(i)\right)\left(x(i-1,t) - m_x(i)\right)}{\sqrt{\sum_{t=0}^{T-1} \left(a(i,t) - m_a(i)\right)^2} \sqrt{\sum_{t=0}^{T-1} \left(x(i-1,t) - m_x(i)\right)^2}} \quad i = 2, N \tag{4}$$

In order to simplify the notation, the mean subtraction step will be implicit in future correlation equations. For ease of calculations, the following substitutions will be used.

$$\begin{aligned} r_i &= \sum_{t=0}^{T-1} a(i,t)x(i-1,t) \\ s_i &= \sum_{t=0}^{T-1} a(i,t)^2 \\ z_i &= \sum_{t=0}^{T-1} x(i-1,t)^2 \\ \rho(i) &= \frac{r_i}{\sqrt{s_i z_i}} \end{aligned} \tag{5}$$

The goal is to force the correlation between $x(i,t)$ and $x(i-1,t)$ to be equal to $\tilde{\rho}(i)$. This correlation can be calculated as follows.

$$\tilde{\rho}(i) = \frac{\sum_{t=0}^{T-1} x(i,t)x(i-1,t)}{\sqrt{\sum_{t=0}^{T-1} x(i,t)^2} \sqrt{\sum_{t=0}^{T-1} x(i-1,t)^2}} \tag{6}$$

To relate this correlation to the scale factor, $b(i)$, we proceed with manipulations of Eq. (3). First, both sides of Eq. (3) are multiplied by $x(i-1,t)$ to give the top equality in Eq. (7). Second, both sides of Eq. (3) are squared to give the middle equality in Eq. (7). This equation is then multiplied by $\sum x(i-1,t)^2$ to yield the lower equality in Eq. (7). Each equality in Eq. (7) is written in terms of the parameters defined in Eq. (5).

$$\begin{aligned}
&\sum_{t=0}^{T-1} x(i,t)x(i-1,t) = \sum_{t=0}^{T-1} a(i,t)x(i-1,t) + b(i)\sum_{t=0}^{T-1} x(i-1,t)^2 = r_i + b(i)z_i \\
&\sum_{t=0}^{T-1} x(i,t)^2 = \sum_{t=0}^{T-1} a(i,t)^2 + 2b(i)\sum_{t=0}^{T-1} a(i,t)x(i-1,t) + b^2(i)\sum_{t=0}^{T-1} x(i-1,t)^2 \\
&\qquad = s_i + 2b(i)r_i + b^2(i)z_i \\
&\sum_{t=0}^{T-1} x(i,t)^2 \sum_{t=0}^{T-1} x(i-1,t)^2 = z_i\left(s_i + 2b(i)r_i + b^2(i)z_i\right) = s_i z_i + 2b(i)r_i z_i + b^2(i){z_i}^2
\end{aligned} \tag{7}$$

Equation (6) can now be re-written as follows.

$$\tilde{\rho}(i) = \frac{\sum_{t=0}^{T-1} x(i,t)x(i-1,t)}{\sqrt{\sum_{t=0}^{T-1} x(i,t)^2 \sum_{t=0}^{T-1} x(i-1,t)^2}} = \frac{r_i + b(i)z_i}{\sqrt{s_i z_i + 2b(i)r_i z_i + b^2(i){z_i}^2}} \tag{8}$$

To obtain the desired correlation, the correct scale factor must be chosen by solving Eq. (8) for $b(i)$. To solve for $b(i)$, both sides of Eq. (8) are squared, the resultant equation is rearranged into a quadratic polynomial, and solved as follows.

$$\tilde{\rho}^2(i) = \frac{r_i^2 + 2b(i)r_i z_i + b^2(i)z_i^2}{s_i z_i + 2b(i)r_i z_i + b^2(i)z_i^2}$$

$$\left(z_i^2(1-\tilde{\rho}^2(i))\right)b^2(i) + \left(2z_i r_i(1-\tilde{\rho}^2(i))\right)b(i) + \left(r_i^2 - s_i z_i \tilde{\rho}^2(i)\right) = 0 \qquad (9)$$

$$b(i) = \frac{-r_i}{z_i} \pm \sqrt{\frac{\tilde{\rho}^2(i)(s_i z_i - r_i^2)}{(1-\tilde{\rho}^2(i))}}$$

If the desired correlation is positive ($\tilde{\rho}(i) > 0$), the maximum value of $b(i)$ is chosen; if the desired correlation is negative ($\tilde{\rho}(i) < 0$), the minimum value of $b(i)$ is chosen. In the discussion given below, the argument of the radical is shown to be non-negative.

At this point, the correlation part of the line scan problem is solved. With $b(i)$ calculated as given in Eq. (9) and following the procedure outlined above culminating in Eq. (3), simulated acoustic noise signals can be created with a correlation coefficient distribution which matches the desired distribution.

C. Matching the Maximum Extreme Value Distribution

A secondary point of emphasis was to force the simulated noise to match the MEV distribution for the measured noise. When using a normal random number generator approach to create simulated acoustic noise signals, the mean of the MEV distribution is controlled by the standard deviation of the random number generator. As discussed below, the mean of the MEV distribution was handled at the end of the correlated noise creation step

by scaling each signal to control the average signal energy. The shape of the MEV distribution depends on the correlation between points in each A-scan; in other words, the shape is controlled by the autocorrelation function or average power spectrum of the noise. As described above, the initial set of uncorrelated noise signals ($a(i,t)\ i=1,N$) are filtered to force an average magnitude spectrum which matches that of the measured noise. The summation process depicted in Eq. (3) alters the average spectrum for the output correlated signals ($x(i,t)\ i=1,N$). Unfortunately, correcting the average spectrum of the correlated signals back to the desired spectrum would alters signal correlations and associated correlation coefficient distribution; thus, motivating the implementation of an iterative approach. The goal is to filter the noise going in to the correlation process so that the noise coming out of the correlation process will have the desired average power spectrum and, therefore, the desired MEV distribution shape.

Additional notation is needed to describe the iterative approach. The output of the correlation process for the k^{th} iteration will be denoted $\mathbf{x}_k = x_k(i,t)\ i=1,N$ with average power spectrum and magnitude spectrum given by $|\mathbf{X}_k(f)|^2$ and $|\mathbf{X}_k(f)|$, respectively. The filters will be denoted $\mathbf{F}_k(f)$ with the initial filter, $\mathbf{F}_1(f)$, based directly in the magnitude spectrum for the measured noise: $\mathbf{F}_1(f)=|\mathbf{X}_m(f)|$. The initial filter, $\mathbf{F}_1(f)$, is the filter used in creating the uncorrelated signals ($\mathbf{a}=a(i,t)\ i=1,N$). The goal is then to make the output spectrum, $|\mathbf{X}_k(f)|$, equal to the desired spectrum, $|\mathbf{X}_m(f)|$, to within some acceptable error. Defining E_x to be the sum of squared errors between $|\mathbf{X}_k(f)|$ and $|\mathbf{X}_m(f)|$ over some frequency range and ε_x to be the acceptable error level, the iterative process will continue

until $E_x \le \varepsilon_x$. The filter is updated after each iteration based on the ratio of the desired and output spectra: $|\mathbf{X}_m(f)|/|\mathbf{X}_k(f)|$.

For a line scan, the iterative approach used to achieve the desired correlation coefficient distribution and frequency spectrum can be summarized in algorithm form as follows:

0. generate a set of white noise signals : $\mathbf{a}_w = a_w(i,t)\ \ i = 1, N$
1. apply the filter, $\mathbf{F}_k(f)$, to the white noise to yield : $\mathbf{a} = a(i,t)\ \ i = 1, N$
2. calculate $\mathbf{x}_k$: $x_k(1,t) = a(1,t)\quad x_k(i,t) = x_k(i-1,t) + b(i)a(i,t)\quad i = 2, N$
3. calculate $|\mathbf{X}_k(f)|$ and the error : $E_x = \sum_{f_i}^{f_f} \left(|\mathbf{X}_m(f)| - |\mathbf{X}_k(f)|\right)^2$
4. if $E_x \le \varepsilon_x$; $\mathbf{x} = \mathbf{x}_k$; stop;
5. if $E_x > \varepsilon_x$; calculate an updated filter : $k = k+1\quad \mathbf{F}_k(f) = \mathbf{F}_{k-1}(f)\dfrac{|\mathbf{X}_m(f)|}{|\mathbf{X}_{k-1}(f)|}$
6. return to step 1.

Empirical evidence shows that the final filter shape is strongly dependent on the desired magnitude spectrum and weakly dependent on the desired conditional correlation coefficient distributions. As such, for a given desired magnitude spectrum, we generally run through the iterative process one time to establish the appropriate filter shape. This filter is then used for all additional runs to generate correlated noise signals, regardless of the desired output correlation coefficient distributions.

Finally, the signals are scaled to achieve the desired mean MEV, that is, the mean MEV associated with the measured acoustic noise signals, denoted m_{mev}. As indicated

earlier, when generating uncorrelated noise signals ($\mathbf{a} = a(i,t)\ i = 1, N$) using a standard normal random number generator with $\sigma = 1$ will force the mean MEV for the signals in **a** to unity. The mean MEV for the correlated noise signals ($\mathbf{x} = x(i,t)\ i = 1, N$) can also be forced to 1 by making the energy of each correlated noise signal equal to the energy of the associated uncorrelated signal. The desired mean MEV can then achieved by scaling by the mean MEV of the measured noise, denoted m_{mev}. This can be done in the computational loop or as a post-processing step as follows: $\mathbf{x} = \mathbf{x}(\sigma_a / \sigma_x) m_{mev}$ where σ_a and σ_x are the standard deviation of the uncorrelated and correlated noise, respectively. Note that scaling the signals does not change the correlation coefficient distribution since the correlation coefficient is scale independent.

We close the section by showing that $b(i)$ is purely real and by considering some special cases. To prove that $b(i)$ will never be imaginary, the value under the square root must be shown to be non-negative. There are three values under the square root $\tilde{\rho}^2(i)$, $(1 - \tilde{\rho}^2(i))$, and $(s_i z_i - r_i^2)$. Since ρ is always between –1 and 1, the first two quantities are clearly greater than or equal to zero. To show that the third quantity is always positive, consider the following manipulations of Eq. (6?), noting that $\tilde{\rho}^2(i) \geq 0$.

$$\rho(i) = \frac{r_i}{\sqrt{s_i z_i}} \quad \Rightarrow \quad r_i^2 = \tilde{\rho}^2(i) s_i z_i \quad \Rightarrow \quad r_i^2 \leq s_i z_i \tag{10}$$

A few special cases should be examined. The first case is where the desired correlation is ± 1. From Eq. (9), it can be seen that setting the desired correlation to ± 1

makes the denominator under the square root equal to 0, forcing $b(i)$ to $\pm\infty$. With reference to Eq. (3), this makes sense because $\tilde{\rho}(i) = \pm 1$ implies $x(i,t) = \pm x(i-1,t)$ which can only be approximated with $b(i) = \pm\infty$ ($a(i,t) \neq 0$). If the desired correlation were ± 1, $x(i,t)$ should simply be set to $\pm x(i-1,t)$.

A second special case would arise if the original correlation (Eq. (5)) were equal to ± 1. For this case, $r_i^2 = s_i z_i$ and the numerator under the radical in Eq. (9) goes to zero. This eliminates the influence of the desired correlation value, $\tilde{\rho}(i)$, and results in $b(i) = -r_i / z_i$. We note from Eq. (8?) that $b(i) = -r_i / z_i \Rightarrow r_i = -b(i) z_i$ will merely set the output correlation to 0. However, when dealing with randomly generated noise, it is exceedingly unlikely that we will come across two signals that have a correlation of 1. If this case were to occur, the problem could be solved by generating a new $a(i,t)$.

D. Two Dimensional Generation of Spatially Correlated Noise

The procedure for generating correlated A-scans which simulate an *xy* raster scan follows directly from the procedure for a line scan. Figure 8 defines some of the notation used in this section. For the two dimensional case, the correlated signals are created in an inner iterative loop with a second outer iterative loop used to simultaneous satisfy the correlation distribution and frequency content requirements. We again begin by assuming that a set of data is taken by measuring backscattered signals at *N x M* equally spaced measurement positions (see Fig. 1). The correlation coefficients between neighboring signals can be used to define the overall and conditional correlation coefficient distributions. These distributions can be used to generate $N(M-1)$ correlation coefficients between signals in a row, denoted $\tilde{\rho}_r(i,j)$, and $(N-1)M$ correlation coefficients between signals in a column,

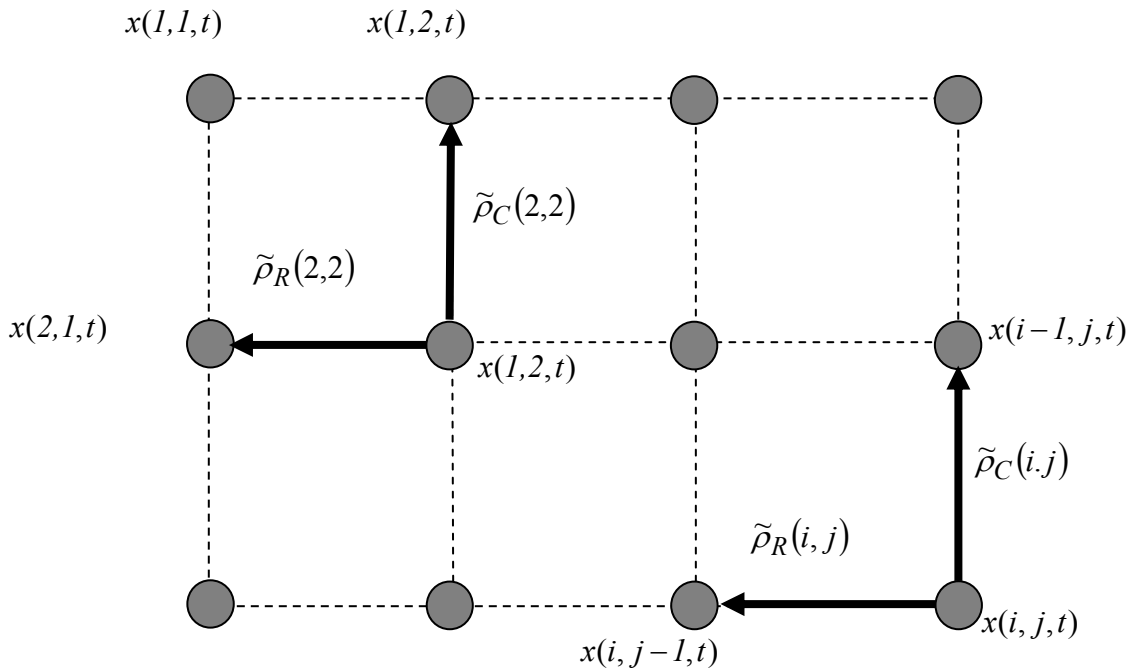

Fig. 8. Representation of the notation and steps involved in creating a simulated raster scan of spatially correlated signals.

denoted $\tilde{\rho}_c(i,j)$. These are the desired correlation values that will be used in determining the scale factors, similarly denoted $b_r(i,j)$ and $b_c(i,j)$. As with the line scan case, desired correlation coefficients can only be drawn from distributions conditioned on correlation coefficient values between previously generated signals.

The procedure again starts with the generation of a set of uncorrelated acoustic noise signals, now written into a thee-dimensional matrix: $\mathbf{a} = a(i,j,t)\ i = 1,N\ \ j = 1,M$. The first row and the first column are treated as line scans. The first output signal, $x(1,1,t)$, is set equal to $a(1,1,t)$. The procedure described above for a line scan is then used to find the scale factors, $b_r(1,j)\ \ j = 2,M$ and $b_c(i,1)\ \ i = 2,N$, and the associated simulated signals, $x(1,j,t)\ \ j = 2,M$ and $x(i,1,t)\ \ i = 2,N$.

The remainder of the correlated signals are created in an iterative fashion starting with $x(2,2,t)$. Each new signal is simultaneously forced toward the desired correlation with two neighboring signals. In general notation (see Fig. 12), $x(i,j,t)$ is iteratively forced toward the desired correlation with $x(i-1,j,t)$ and $x(i,j-1,t)$ by using the sum of appropriately scaled versions of these two signals plus $a(i,j,t)$.

To generate the signal $x(i,j,t)$, the algorithmic loop can be summarized as follows:

1. Calculate the scale factors required to force the desired correlation between $x(i,j,t)$ and $x(i-1,j,t)$, denoted $\tilde{\rho}_c(i,j)$, and between $x(i,j,t)$ and $x(i,j-1,t)$, denoted $\tilde{\rho}_r(i,j)$:

$$b_c(i,j) = \frac{-r_{cij}}{z_{cij}} \pm \sqrt{\frac{\tilde{\rho}_c^2(i,j)(s_{cij}z_{cij} - r_{cij}^2)}{(1-\tilde{\rho}_c^2(i,j))}}$$

$$b_r(i,j) = \frac{-r_{rij}}{z_{rij}} \pm \sqrt{\frac{\tilde{\rho}_r^2(i,j)(s_{rij}z_{rij} - r_{rij}^2)}{(1-\tilde{\rho}_r^2(i,j))}} \qquad (11)$$

2. Calculate the output signal using both scale factors and all three signals:

$$x(i,j,t) = a(i,j,t) + b_r(i,j,)x(i,j-1,t) + b_c(i,j)x(i-1,j,t) \qquad (12)$$

3. Calculated the actual correlation coefficient between $x(i,j,t)$ and $x(i-1,j,t)$,denoted $\bar{\rho}_c(i,j)$, and between $x(i,j,t)$ and $x(i,j-1,t)$, denoted $\bar{\rho}_r(i,j)$,

$$\bar{\rho}_c(i,j) = \frac{\sum_{t=0}^{T-1} x(i,j,t)x(i-1,j,t)}{\sqrt{\sum_{t=0}^{T-1} x(i,j,t)^2}\sqrt{\sum_{t=0}^{T-1} x(i-1,j,t)^2}}$$

$$\bar{\rho}_r(i,j) = \frac{\sum_{t=0}^{T-1} x(i,j,t)x(i,j-1,t)}{\sqrt{\sum_{t=0}^{T-1} x(i,j,t)^2}\sqrt{\sum_{t=0}^{T-1} x(i,j-1,t)^2}} \qquad (13)$$

4. Calculate the correlation coefficient error and compare with the acceptable error level, ε_ρ:

$$\delta\rho_c(i,j) = \left|\tilde{\rho}_c(i,j) - \bar{\rho}_c(i,j)\right| \qquad \delta\rho_r(i,j) = \left|\tilde{\rho}_r(i,j) - \bar{\rho}_r(i,j)\right| \qquad (14)$$

   If $\delta\rho_c(i,j) \le \varepsilon_\rho$ *and* $\delta\rho_r(i,j) \le \varepsilon_\rho$ then stop; else go to step 5.

5. Use the current output signal as a new starting signal: $a(i,j,t) = x(i,j,t)$. Return to step 1.

The loop is repeated until $NM - (N+M)$ correlated acoustic noise signals have been generated. Note that $x(i,j,t)$ is correlated with each of its four neighbors since $x(i,j,t)$ is calculated based on its correlation with $x(i-1,j,t)$ and $x(i,j-1,t)$, and $x(i+1,j,t)$ and $x(i,j+1,t)$ are calculated based on their correlations with $x(i,j,t)$ (see Fig. 8).

Finally, the MEV distribution shape and position are addressed. As with the line scan, an outer iterative loop is used to force the generated signals to have the desired frequency content, and thus the MEV distribution shape, while maintaining the desired correlation coefficient distribution. This iterative process follows directly from the steps outlined for a line scan in the previous section with only notational changes required to account for three-dimensional rather than two-dimensional matrices. The position of the MEV distribution for the simulated signals is again dealt with by scaling of the simulated signals, following the approach outlined for the line scan: $\mathbf{x} = \mathbf{x}(\sigma_a / \sigma_x) m_{mev}$.

IV. Results

A. Implementation

The MEV distributions (Fig. 1) and conditional correlation coefficient distributions associated with the overall distributions shown in Fig. 3 were used as the desired distributions to demonstrate implementation of the noise generation approach. A periodogram approach was used to estimate the average magnitude spectrum of the measured noise for use in creating acoustic noise signals with the desired MEV distribution shape. Desired correlation coefficients were drawn from interpolation-based conditional probability density functions which were based on conditional histograms constructed from the measured noise. Spatially correlated acoustic noise A-scans, each 51 points long, were generated to simulate a 50 x 50 raster scan at a digitization rate of 100 MS/s (10 ns/point).

B. Results

We begin by showing an example of the evolution of correlation coefficients and signals toward the desired result for the middle distribution shown in Fig. 3. The two dashed lines in Fig. 9 show examples of the how the actual correlation values, $\bar{\rho}_r(i, j)$ and $\bar{\rho}_c(i, j)$,

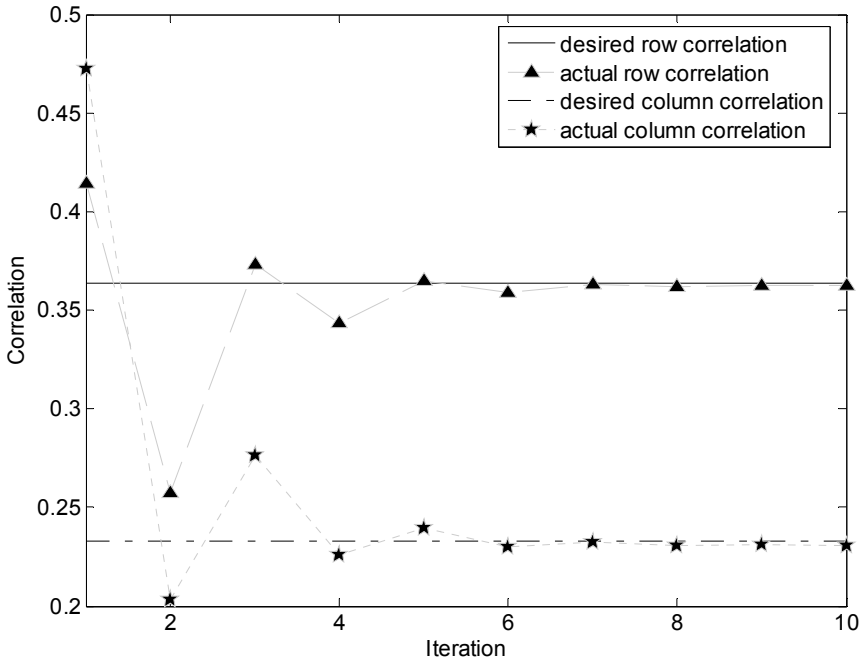

Fig. 9. Example of the progression of row (upper) and column (lower) correlation coefficients toward the desired values during the iterative process.

move toward the desired values, $\tilde{\rho}_r(i,j)$ and $\tilde{\rho}_c(i,j)$, with each iteration. Figure 10 shows how one uncorrelated noise signal, $a(i,j)$ (solid lines, upper graphs), can start at an arbitrary correlation coefficients with its neighboring signals (dashed lines in the upper and lower graphs) and then after iteration evolve to a correlated noise signal, $x(i,j)$ (solid lines, lower graphs), showing the desired correlations with its neighbors.

The method outlined for creating correlated noise was tested for each of the overall correlation coefficient distributions shown in Fig. 3. Given the stochastic nature of this problem, each time a set of correlated noise signals is generated, the resultant histograms represent one realization of noise generation process. In this section, we show example histograms for one realization of the process, and we give chi-squared analysis results that quantify the average agreement between the desired and output histograms.

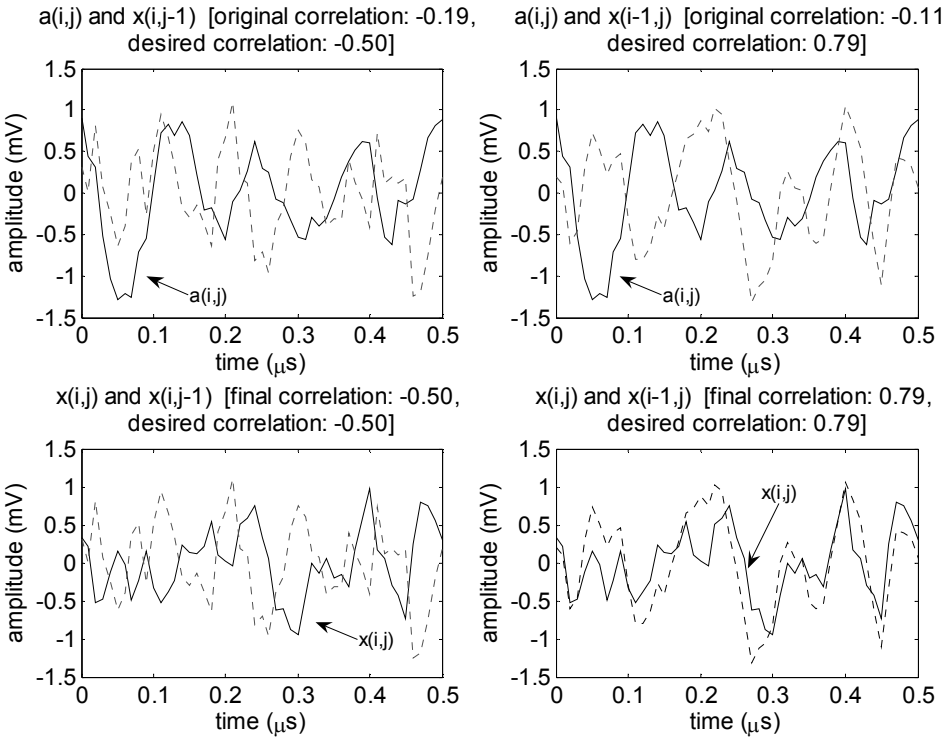

Fig. 10. Example of a signal, initially having arbitrary correlations with adjacent signals, evolving during the iterative process to have the desired correlations with the adjacent signals. The top row shows the original signal to be modified (solid lines) along the adjacent signals (dashed lines). After the iterative process, the final modified signal (solid line) is shown with the adjacent signals (dashed lines).

Desired and actual histograms are given in Fig. 11 for overall correlation coefficient distributions and in Fig. 12 for the MEV distributions. The histograms in each figure show the desired correlation distributions (Fig. 3) and MEV distributions (Fig. 1). The star data points superimposed on the histograms represent the bin values for the histograms determined from the simulated noise. For each distribution, signals were generated to simulate a 50 x 50 scan, yielding 2500 signals, and 4900 nearest-neighbor correlations. The success of the approach is witnessed by the agreement between the histograms for measured

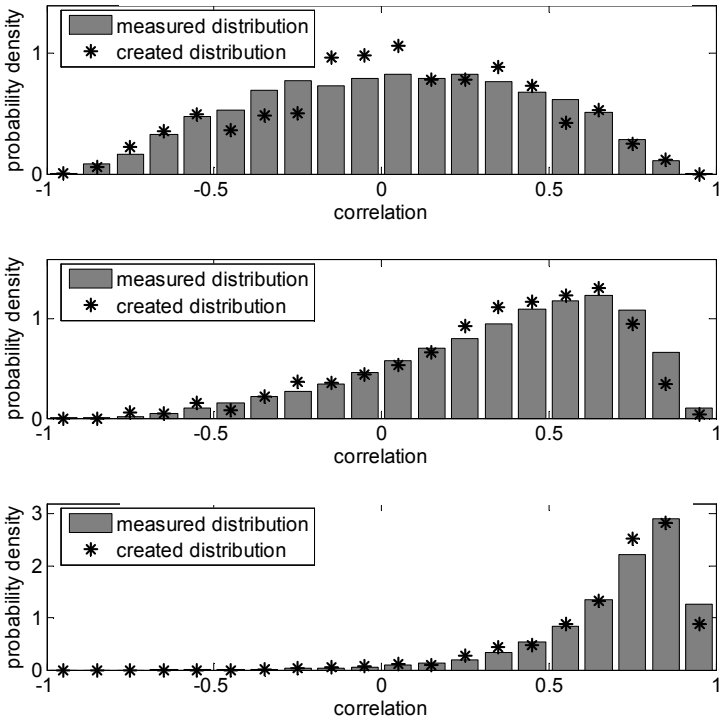

Fig. 11. Example histograms of spatial correlation coefficients for measured and simulated noise signals at 2 mm (upper), 1 mm (middle), and 0.5 mm (lower) measurement position spacing.

and created noise signals. Again note that each set of simulated signals will give a slightly different correlation coefficient histograms and MEV distributions.

The results were also evaluated quantitatively using a chi-squared test. The test is based on the agreement between histogram bin values associated with the generated and measured noise, with the measured-noise based histograms representing the desired values. Using the vector h_c and h_m to hold the bin values for the calculated and measured noise, respectively, the chi squared error between the two histograms can be written as follows:

$$\chi^2 = \sum_{1}^{k} \frac{(h_m - h_c)^2}{h_m} \tag{15}$$

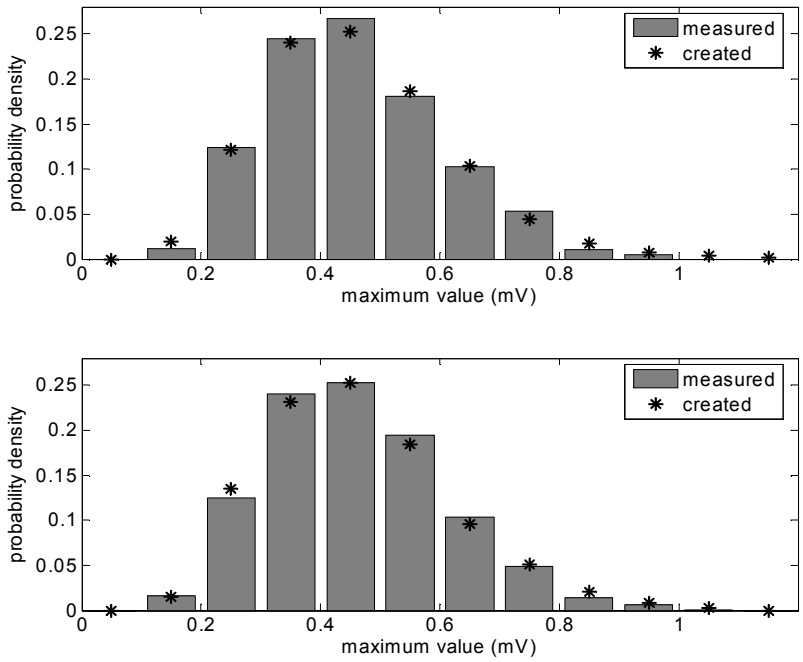

Fig. 12. Example histograms of maximum extreme values for measured and simulated noise signals at 1.5 mm (upper) and 0.5 mm (lower) measurement position spacing.

where k represents the number of bins. This statistic was looked up in a standard chi squared table with $k-1$ degrees of freedom. The resulting p-value is the probability that the same error would result if both histograms were indeed from the same distribution. Thus if we pick a cutoff value, such as 0.05, any p value above this cutoff is deemed acceptable.

This process was done on 10 sets of 20 x 20 of simulated noise. For the MEV histogram shown in Fig. 1, the average p-value was 0.325, with a standard deviation of 0.233. For the overall correlation histogram, the average p-value was 0.557, with a standard deviation of 0.340. For the conditional correlation histogram, the average p-value was 0.220 with a standard deviation of 0.404. These quantitative results indicate that on the average for MEV, overall correlation, and conditional correlation distribution, the distributions for the simulated noise are consistent with the desired distributions based on the measured noise.

V. Summary

An approach has been outlined for generating simulated acoustic noise with a correlation coefficient distribution and MEV distribution which matches those distributions for measured acoustic noise. With this approach, a limited number of measured signals can be used to establish the correlation coefficient and MEV distributions which drive the computer generation of a large number of simulated acoustic noise signals. Signals simulated in this manner are being used in the development of a scale independent correlation based approach to defect detection.[7,8]

Acknowledgements

This work was supported by the Center for Aerospace Manufacturing Technology (CAMT) at the University of Missouri-Rolla funded under Air Force Research Laboratory Contract FA8650-04-C-5704 and by Boeing under PO Z40791. Previous support for development of the correlation approach was provided by Honeywell Federal Manufacturing and Technology and by the National Science Foundation (NSF CMS 9610189). The authors would like to acknowledge early development work on correlation analysis by previous postdocs and students including Dr. Mark D. Russell, Dr. Terence P. Lerch, and Brett Rinker. The authors would also like to acknowledge the tremendous support from personnel at Honeywell FM&T including Eric Jamieson, Jose A. Samayoa, Jason P. Miller and Brett Rinker. In particular, the encouragement by Eric Jamieson to extent the correlation approach to localized flaw detection was pivotal. Many thanks are also due to Dr. Zoughi from the University of Missouri-Rolla and Dr. Palmer from the Boeing Company Phantom Works for their technical guidance and leadership.

References

1. R. B. Thompson, L. Yu, and F. J. Margetan, "A formal theory for the spatial correlation of backscattered ultrasonic grain noise", *Review of Progress in Quantitative Nondestructive Evaluation*, Vol. 24, edited by D. E. Chimenti and D. O. Thompson, AIP, Melville, 2005, pp. 1292-1299.

2. F. J. Margetan, E. Nieters, L. Brasche, L. Yu, A. Degtyar, H. Wasan, M. Keller, and A. Kinney, "Fundamental Studies of Titanium Forging Materials - Engine Titanium Consortium II", FAA William J. Hughes Technical Center, Atlantic City, N. J., Report number DOT/FAA/AR-05/22 (June 2005).

3. A. Dogandzic and N. Eua-Anant, "Defect detection in correlated noise", *Review of Progress in Quantitative Nondestructive Evaluation*, Vol. 23A, edited by D. E. Chimenti and D. O. Thompson, AIP, Melville, 2004, pp. 628-635.

4. W. F. Walker, "The significance of correlation in ultrasound signal processing", *Proc. SPIE Vol. 4325, Medical Imaging: Ultrasonic Imaging and Signal Processing*, edited by Michael F. Insana and K. Kirk Shung, 2001, pp. 159-171.

5. J. S. Bendat and A. G. Piersol, *Engineering Applications of Correlation and Spectral Analysis*, J. Wiley, New York, p. 46, 1993.

6. P. B. Nagy and L. Adler, "Ultrasonic NDE of Solid State Bonds: Inertia and Friction Welds", *J. Nondestructive Eval*. **7(3/4)**, 199-215, (1988).

7. B. A. Rinker, E. E. Jamieson, J. A. Samayoa, T. G. Abeln, T. P. Lerch, and S. P. Neal, "Detection of weak interface signals for same material bond/weld inspection", *Review of Progress in Quantitative Nondestructive Evaluation*, Vol. 22B, edited by D. E. Chimenti and D. O. Thompson, AIP, Melville, 2003, pp. 1080-1087.

8. R. Cepel, D. O. Palmer, Jr., and S. P. Neal, "A preliminary study of ultrasonic detection of cracks through thick composite doublers", *Proceedings of the 9th Joint FAA/DOD/NASA Conference on Aging Aircraft*, Atlanta, GA, March 6-9, 2006.

9. C. S. Padgett, L. A. Thombs, and W. J. Padgett, "On the α-risks for Shewhart control charts", *Communications in Statistics, Part B -- Simulation and Computation*, **21**, 1125-1147, (1992).

10. P. I. Brooker, "Simulation of spatially correlated data in two dimensions", *Mathematics and Computers in Simulation*, **27**, 155-157, (1985).

11. N. Cressie, *Statistics for Spatial Data*, J. Wiley, New York, (1991).

12. P. C. Kyriakidis, N. L. Miller, and J. Kim, "A Spatial Time Series framework for simulation daily precipitation at regional scales," *Journal of Hydrology,* **297**, 236-255, (2004).

13. MATLAB version 7.0.0. The MathWorks, Inc., Natick, Massachusetts, (2004).

CHAPTER 4
A QUANTATIVE ANALYSIS OF THE USE OF SPATIAL CROSS-CORRELATION FOR FLAW DETECTION

by

Raina Cepel, Dominic Ho, and Steven P. Neal

Abstract:

The use of the spatial cross correlation coefficient between adjacent windowed A-scans has been proposed as a flaw detection method to complement gated peak detection and matched filtering. To quantitatively compare the methods, grain noise and noise-corrupted flaw signals are simulated under varying conditions. Receiver operating characteristic curves are calculated for each detection statistic and the area under the curve is used to compare performance. The spatial cross correlation approach is found to outperform gated peak detection at low signal to noise ratios. When the *a priori* flaw signal prediction is inadequate, the correlation approach also outperforms matched filtering. Techniques to maximize the efficacy of the spatial cross correlation approach are suggested.

I. Introduction

The typical flaw detection method used in ultrasonic nondestructive evaluation (NDE) is gated peak-detection. The statistic used for this approach is either the maximum absolute value or the maximum peak to peak value of a voltage versus time signal, called an A-scan. An image of these values plotted versus their corresponding lateral spatial positions is called a C-scan. From here, a simple threshold can be applied to the image for flaw detection. Image processing techniques can also be applied to the C-scan in order to enhance flaw detection. This approach is inherently amplitude dependent, thus is effective at high signal to noise ratios (SNR), but exhibits poor performance at low SNR where flaw signals have amplitudes on the order of the background noise.

Matched filtering is another detection technique [1,2] that filters each received signal with a template that is chosen by the user to be the best match to the expected flaw signal. In effect, matched filtering correlates each measured A-scan with the template. This approach is amplitude independent and as such has the capability to be effective at low SNR, but only when an accurate prediction of the flaw signal is used. In instances where the template is significantly different from the flaw signals, the performance of matched filtering degrades. Previous work on the use of matched filter for ultrasonic defect detection by Xin et al. [3], Chiou et al. [4], and Srinivasan et al. [5] addresses the difficulties in estimating the template along with the use of model-based approaches for template estimation.

The spatial cross-correlation coefficient between adjacent A-scans [6,7] has been proposed as a complementary detection statistic[8-10]. The new method uses the same A-scans from which the gated peak-detection and matched filtering statistics are calculated. The detection statistic is calculated as the cross-correlation between each pair of adjacent

gated A-scans. These values can be formed into an image which is qualitatively similar to the C-scan image [9,10]. Like the matched filter approach, the correlation approach is amplitude independent, relying instead on the similarity of signals. However, unlike matched filtering, the spatial cross-correlation coefficient does not require the prediction of an *a priori* estimate of the flaw signal template. Instead, each signal is essentially used as a matched filtering template for each of its neighbors.

To quantitatively compare the performance of the spatial cross-correlation method to the gated peak-detection and matched filtering approaches, simulated grain noise and noise-corrupted flaw signals are created under varying conditions. For each set of conditions, a receiver operating characteristic curve is calculated for each detection statistic and the area under the curve is used as a basis for comparing each detection approach. Some conclusions are made about under which circumstances the use of spatial cross-correlation should be considered, and recommendations are made to aid in maximizing the efficacy of this detection approach given certain invariant experimental conditions.

II. Measurement Procedure

Several sets of ultrasonic data were measured and used as a basis for the simulation. The ultrasonic measurement system that was used in these measurements consists of a water tank filled with degassed tap water at approximately 19°C, a three dimensional scanning bridge that holds the transducer, a pulser-receiver unit, and a 12 bit data acquisition card with a sample rate of 100 MS/s. A PC collects data from the acquisition card and controls the motor controller that moves the scanning bridge. A leveling plate was used to ensure that the specimen was aligned with the scan plane of the transducer and the transducer face was also

normalized in relation to the scan plane. At each measurement position, 64 signals were taken and averaged together in order to reduce electronic noise.

The first set of data collected consists of backscattered grain noise signals from a stainless steel plate with the dimensions 10.1 x 5 x 1.9 cm. Signals were taken over a 3.2 x 2.4 cm grid with 0.5 mm between measurement positions. The pulser-receiver and data acquisition card settings were chosen such that the front and back surface reflections were larger than the digitization range and the grain noise was properly digitized. The transducer used to make these measurements was a focused ½" diameter transducer with a 10 MHz center frequency and a 4" focal length. The water path of the transducer was chosen such that the focal zone was at the approximate mid-plane of the sample.

The second set of data collected was from a piece of 60 grit sandpaper of the dimensions 6 x 6 cm sandwiched between two pieces of Plexiglas. Signals were taken over a 5 x 5 cm grid with 0.25 mm between measurement positions. The same ½" diameter focused transducer with a 10 MHz center frequency and a 4" focal length was used. The water path of the transducer was chosen such that the focal zone was at the approximate mid-plane of the sample.

The third set of data collected was from a copper plate with the dimensions 7.5 x 7.5 x .5 cm. Signals were taken over a 1 x 1 cm grid with 1 mm between measurement positions. The transducer used to make these measurements was a focused ½" diameter transducer with a 15 MHz center frequency and a 3" focal length, with the focal zone not at any particular plane. For both of these sets of data, the pulsar-receiver and data acquisition card settings were chosen such that the front and back surface reflections were within the digitization range.

III. Detection Statistics and Simulated Grain Noise

The goal of the simulation and ROC analysis given below is to quantitatively compare the performance of the proposed spatial cross-correlation approach to the classical gated-peak detection method and to matched filtering. This section describes each detection statistic in detail.

The first detection statistic is the maximum extreme value, or MEV, which is a commonly used type of gated peak-detection that is found by taking the maximum of the absolute value of each gated A-scan. Often a threshold value is chosen based on calibration experiments, and any signal that breaches that threshold is deemed to contain a flaw. A spatial image of these values is called a C-scan and can be used for flaw detection.

Creating realistic simulated grain noise to be used in an analysis of the MEV statistic is a relatively simple procedure. A standard normal random noise generator is used to create a time domain white noise signal which is then filtered based on the frequency spectrum of the measured grain noise. This procedure is repeated independently at each measurement position. A detailed discussion of the computer generation of grain noise whose MEV distribution matches that of measured grain noise is given in Ch. 2.

The new detection statistic is the spatial cross-correlation coefficient. This statistic is found by calculating the correlation coefficient between gated A-scans at adjacent measurement positions. Consider an *N x M* scan with each A-scan *T* points long and using the array $z = z_{i,j}(t)\ \ i = 1...N\ \ \ j = 1...M\ \ \ t = 0...T-1$ to hold the A-scans. Calculation of the correlation coefficient between A-scans is then given by the following equation where $\hat{\rho} = \hat{\rho}(i, j, \delta_r, \delta_c, \tau)$ is a sample estimate of the associated expected value:

$$\hat{\rho} = \frac{\sum_{t=t_i}^{t_f} \left(z_{i,j}\left(t-\tau\right) - m_{i,j} \right) \left(z_{i+\delta_c, j+\delta_r}\left(t\right) - m_{i+\delta_c, j+\delta_r} \right)}{\sqrt{\sum_{t=t_i}^{t_f} \left(z_{i,j}\left(t-\tau\right) - m_{i,j} \right)^2} \sqrt{\sum_{t=t_i}^{t_f} \left(z_{i+\delta_c, j+\delta_r}\left(t\right) - m_{i+\delta_c, j+\delta_r} \right)^2}} \qquad (1)$$

Normalization removes the scale dependence and restricts $\hat{\rho}$ to the range -1 to 1. In Eq. (1), the summation range in the time-domain defines the portion of the signal (the time window or gate) of interest, m is the mean value calculated over the gate, τ controls the lag or temporal shift between the two signals, and δ is a spatial shift parameter. Throughout the paper, t is used as a discrete index referring to the temporal direction. With $\delta_r = 1,\ \delta_c = 0$, "row correlations" are calculated between adjacent A-scans, that is, A-scans measured at the j^{th} and $j^{th}+1$ positions in the i^{th} scan row. Similarly, with $\delta_r = 0,\ \delta_c = 1$, "column correlations" can be calculated. These correlation values can be formed into an image comparable to the C-scan. A discussion of the procedure for forming an image is given in Ch. 1.

Creating realistic simulated grain noise to be used in an analysis of the spatial cross correlation coefficient is a more complex procedure. A detailed discussion of the computer generation of grain noise with a given MEV distribution is given in Ch. 2. Because the correlation coefficient measures the similarity of two adjacent signals, it can no longer be assumed that noise at any one measurement position is independent of its neighbors. Experiments show that below a certain measurement spacing, adjacent grain noise signals have an average correlation coefficient greater than zero [11,12]. Physically this is due to the fact that the grain noise signal is created by the reflections from many small grains over the

volume that is within the beam field of the transducer. Thus when the transducer moves only a small amount, some of the same grains that contributed to the grain noise at the adjacent location will still be within the transducers beam field at the new location. Any simulation that attempts to accurately evaluate the efficacy of the correlation coefficient statistic must use simulated grain noise whose underlying spatial cross correlation coefficient distribution matches that of the measured grain noise being used as a template. In each measurement position a grain noise signal, $x(i, j, t)$, is calculated as a weighted sum of a randomly generated signal, $a(i, j, t)$, and the previously created signals in adjacent measurement positions.

$$x(i, j, t) = a(i, j, t) + b_r(i, j)x(i, j-1, t) + b_c(i, j)x(i-1, j, t) \qquad (2)$$

The weights, b_r and b_c, are independently calculated for each neighboring signal by algebraic manipulation of the correlation coefficient equation. Applying this procedure iteratively results in a noise signal that has a specified cross correlation with each of its neighbors. The specified cross correlations are drawn from the correlation coefficient distribution of the measured grain noise. Previous work by Cepel et al. [10] describes this procedure for creating spatially correlated grain noise in more detail including the calculation of the statistics of the measured grain noise, the procedure for creating the randomly generated signals, $a(i, j, t)$, the equations for the weights, b_r and b_c, the iterative algorithm to create the correlated grain noise itself, and the method for ensuring that the created noise also matches the MEV distribution of the measured noise.

Spatial cross correlation is comparable to matched filtering. For matched filtering, the expected flaw signal, $s_i^m(t)$, is correlated with each gated A-scan, which consists of a flaw signal and grain noise, $s_i(t)+n_i(t)$. The maximum value of the resulting signal is used as a detection statistic.

$$\beta_m(\tau)=\sum s_i^m(t-\tau)x_i(t)=\sum_t s_i^m(t-\tau)s_i(t)+\sum_t s_i^m(t-\tau)n_i(t) \qquad (3)$$

$$= \quad \alpha_m \quad + \quad \alpha_n$$

Here β_m is the matched filter output and we assume that the flaw signals all have unit energy and that all processes are zero mean. The variable τ sweeps the matched filter over the A-scan in time. The maximum value of $\beta_m(\tau)$ is used as the matched filter detection statistic. A measure of the quality of the matched filter template is given by the similarity in $s_i^m(t)$ and $s_i(t)$ as quantified by α_m. Given the unit energy assumption, $\alpha_m=1$ for the ideal case where $s_i^m(t)=s_i(t)$. Under these circumstances, matched filtering will always perform better than correlation because there is noise in only one of the two signals being used for each correlation calculation. However, in cases where the expected flaw signal does not equal the actual flaw signal, $\alpha_m<1$, and the spatial cross-correlation approach may perform better than matched filtering. A more robust mathematical comparison between matched filtering and spatial cross correlation is found in [10] (se Ch. 1). The same grain noise signals that are used for analysis of the cross-correlation statistic can be used for analysis of the matched filtering statistic.

IV. Simulation and ROC Analysis

Simulated grain noise signals and flaw signals corrupted with grain noise were used to facilitate the quantitative comparison of the three detection statistics using receiver operating characteristic (ROC) analysis. A robust ROC analysis requires an accurate distribution of each statistic, both with and without the presence of a flaw signal. Because it is difficult to collect experimental data ranging over all possible conditions, a simulation is advantageous in that it allows the creation of a large number of signals under varying measurement and analysis conditions. This section addresses the formation of noise-corrupted flaw signals and describes the conditions varied during ROC analysis.

The creation of grain noise signals was dealt with briefly in this previous section. To create noise-corrupted flaw signals, Gaussian damped sinusoids were used to simulate defect signals with the desired frequency content, which matched the frequency content of the grain noise. In some cases, experimental data was used directly to simulate flaw signals. To simulate defects with variable aspect ratios and at variable signal to noise ratios, the defect signals were scaled over certain spatial regions and added to the simulated grain noise signals. This process is represented in equation form for a signal measured at the *ij* position in a simulated raster scan:

$$x(i,j,t) = n(i,j,t) + B(i,j)y(t - \tau(i,j)) \tag{4}$$

where $x(i,j,t)$ is the final noise-corrupted defect signal, $y(i,j,t)$ is the flaw signal, and $n(i,j,t)$ represents the simulated grain noise with unity power, which was generated to mimic the maximum extreme value (gated peak value) distribution and correlation

coefficient distribution associated with measured noise. Flaw signals can be shifted in time relative to one another with $\tau(i,j)$. The SNR at each *ij* position is controlled by $B(i,j)$, a scale factor which can be varied over lateral space.

A ROC based comparison of the spatial cross-correlation with gated peak-detection was done over a more complete set of variable conditions than for the comparison between the correlation approaches and matched filtering. This was done because the relative performance of the correlation and gated peak-detection approaches varies significantly with a large number of conditions, whereas the performance of the matched filtering approach depends largely on the accuracy of the template used, and very little on any other variables.

Measurement conditions, which are controlled by the experimental set-up and sample characteristics, were simulated. The following measurement conditions were varied during the simulation: 1) SNR was varied by weighting the flaw signals with $B(i,j)$. 2) The measurement spacing between simulated grain noise signals was varied, based on measured noise that was collected at variable measurement spacings. 3) Lateral flaw size was varied using $B(i,j)$, whose values were set to vary with lateral space. At each *ij* location where B is non-zero, a noise-corrupted flaw signal is created, and at each *ij* location where B is set to zero, the signal contains only noise. 4) The misalignment of adjacent flaw signals in time (i.e., a phase shift) was achieved by varying $\tau(i,j)$ over lateral space. 5) Flaw signals were varied over lateral space such that $y(i,j,t) \neq y(i+\delta_r, j+\delta_c, t)$. 6) The value of α_m, which quantifies the similarity between the matched filter template and the flaw signal, was varied. Analysis conditions, or the settings that control the analysis of the data, were also varied as follows: 7) The maximum value of τ, the time shifting parameter used to calculate the

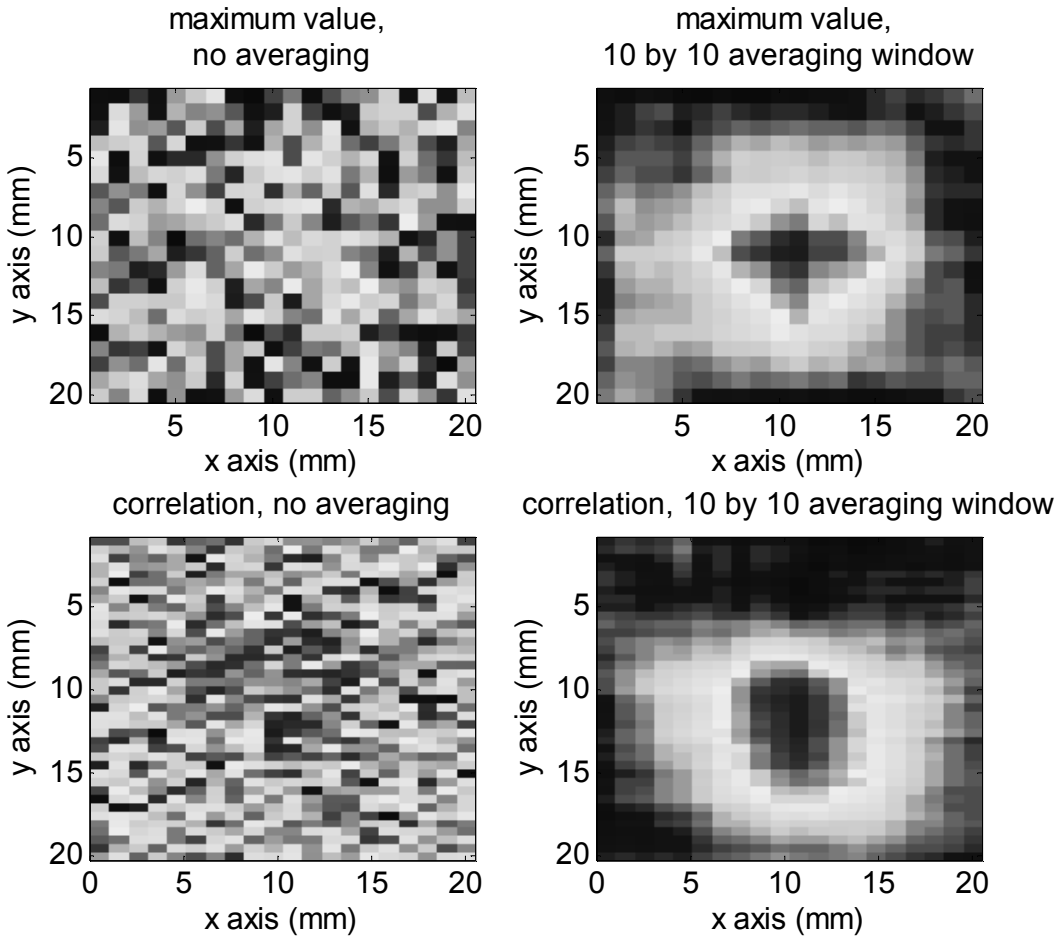

Fig. 1. The effects of spatial averaging are shown in this figure. The top left panel shows a C-scan image containing a difficult to see flaw. In the top right panel, spatial averaging using a 10 by 10 window size has been applied and the flaw is clearly apparent. The bottom left panel shows an image of correlation-coefficients, and the bottom right panel again shows the image after the application of spatial averaging.

spatial cross-correlation in Eq. (1), was allowed to vary. 8) Spatial averaging, a common image processing technique [13] where each individual statistic is averaged with a number of adjacent neighbors, was applied with the number of statistics averaged over lateral space variable. Figure 1 shows an example of spatial averaging. The top left panel shows a C-scan containing a flaw that is difficult to discern from the background noise. The application of a 10 x 10 averaging window, which averages 100 statistics together in each lateral position, is

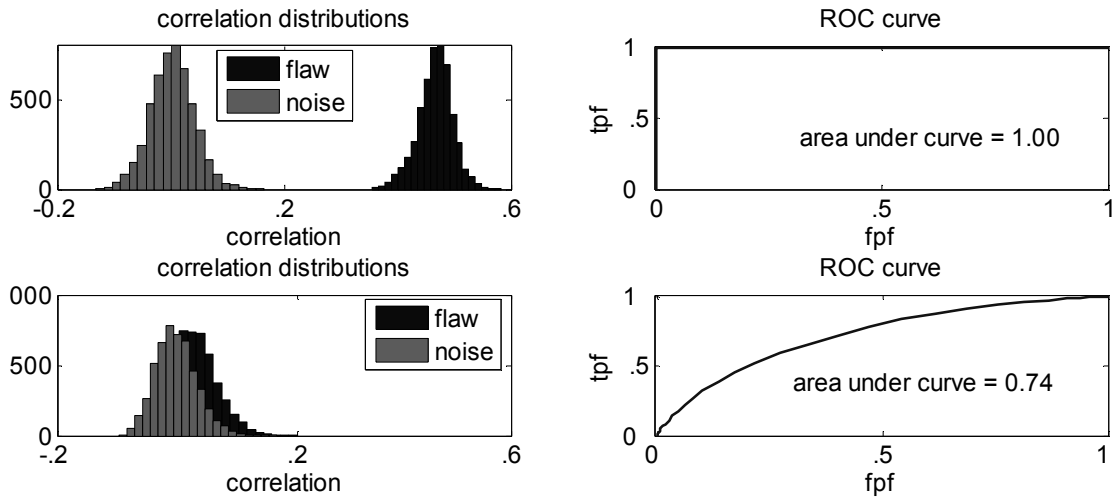

Fig. 2. The use of Receiver Operating Characteristic (ROC) curves. The top left distribution shows a noise and noise + flaw distribution that are well separated. The ROC curve on the top right plots the true positive fraction (TPF), or fraction of noise-corrupted flaw signals that would be accurately characterized as containing a flaw, versus the false positive fraction (FPF), or fraction of noise signals that would be inaccurately characterized as containing a flaw. Because the distributions are well separated, the ROC curve is ideal and the area beneath it is one. In the bottom left panel, the distributions overlap significantly and the ROC curve in the bottom right panel reflects this, resulting in a small area beneath the curve.

shown in the top right panel, where the flaw is now easily seen. A similar procedure is shown in the lower panels with the correlation statistic.

Receiver operating characteristic curves [14] were used to provide a quantitative measure of the effectiveness of each signal at differentiating noise corrupted flaw signals from grain noise signals. Qualitatively, the set of distributions, one for noise-corrupted flaw signals and one for noise signals, in the top left panel of Figure 2 look more separated than the set of distributions in the bottom left panel. ROC curves based on these sets of distributions have been calculated and are shown on the right. The detection threshold is varied over its range of possible values, and at each point the true positive fraction (TPF), or fraction of noise-corrupted flaw signals that would be accurately characterized as containing a flaw, is plotted versus the false positive fraction (FPF), or fraction of noise signals that

would be inaccurately characterized as containing a flaw. The area under the ROC curve can be used as a single value to compare two sets of distributions. When the distributions are completely separated, the ROC curve is ideal and the area under it is unity. When the distributions overlap, the area under the ROC curve is between 0.5 and 1, reflecting the tradeoff between missed flaw detections and false calls.

The simulation creates two sets of signals, one set that contain only grain noise and one set that contain flaw signals and grain noise. The detection statistics are computed for each case and the noise and noise-corrupted flaw distributions are compared using ROC analysis. In the results section, the area under the ROC curve is plotted versus the variable being investigated for each detection statistic.

V. Results

The results section compares the performance of the newly proposed spatial cross-correlation approach with gated peak-detection and with matched filtering, using the area under the ROC curve as a basis of comparison. This analysis is intended to help guide decisions as to under what conditions it might be advantageous to use the correlation based approach in addition to alternative techniques. Additionally, the analysis aims to provide guidance as to how the measurement and analysis variables should be chosen to maximize the benefit of the correlation approach.

A. Comparison of Cross-Correlation and Gated Peak-Detection

The first condition varied was the signal to noise ratio, which was changed by scaling the flaw signals with $B(i,j)$ before the grain noise was added, while the measurement spacing of the grain noise was held constant at 1.75 mm. The value of $\tau(i,j)$ was held

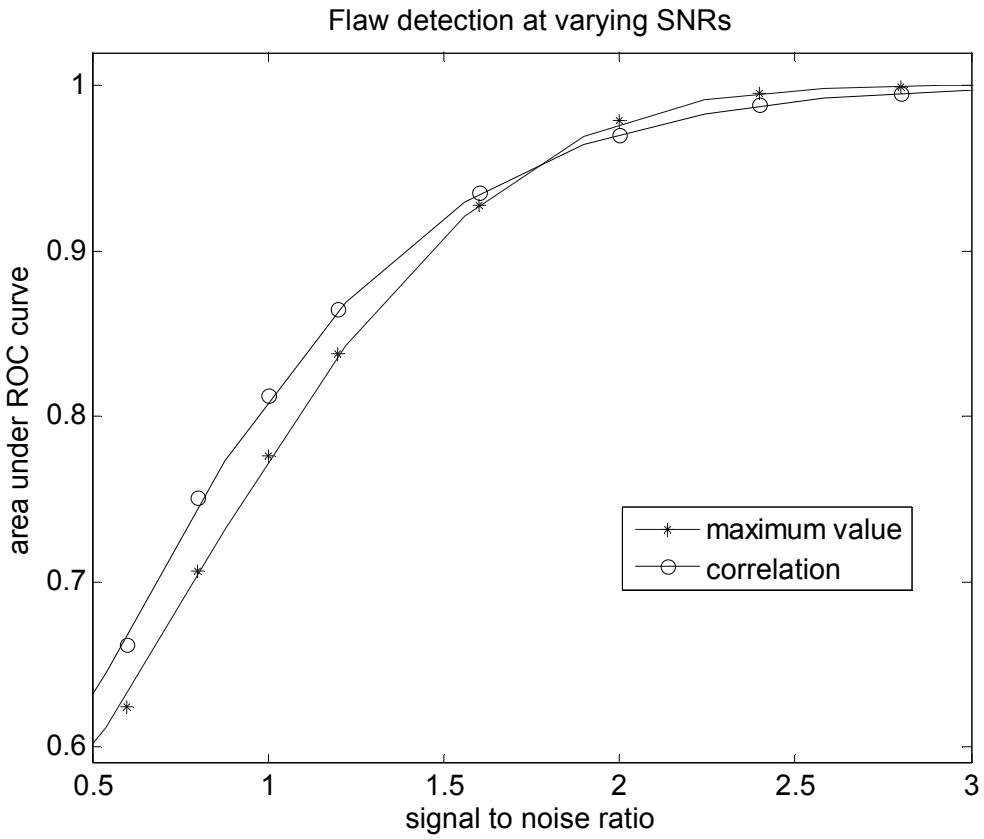

Fig. 3. The area under the ROC curve of the maximum value and correlation statistics as the signal to noise ratio varies. Measurement spacing is held constant at 1.75 mm, flaw size is infinite, and no misalignment, averaging, or realignment is done.

constant at zero, $B(i,j)$ and $y(i,j,t)$ were held constant over lateral space, and no averaging or realignment was done during analysis. The results are shown in Figure 3, where "correlation" refers to the spatial cross-correlation statistic and "maximum value" refers to the maximum extreme value statistic, which is a type of gated peak-detection. A cubic spline has been fit through the data points for visualization purposes. The SNR is plotted on the x-axis and was calculated as the ratio of the extreme value of the flaw signal to the average extreme value of the grain noise signals. The figure shows that as the SNR increases the

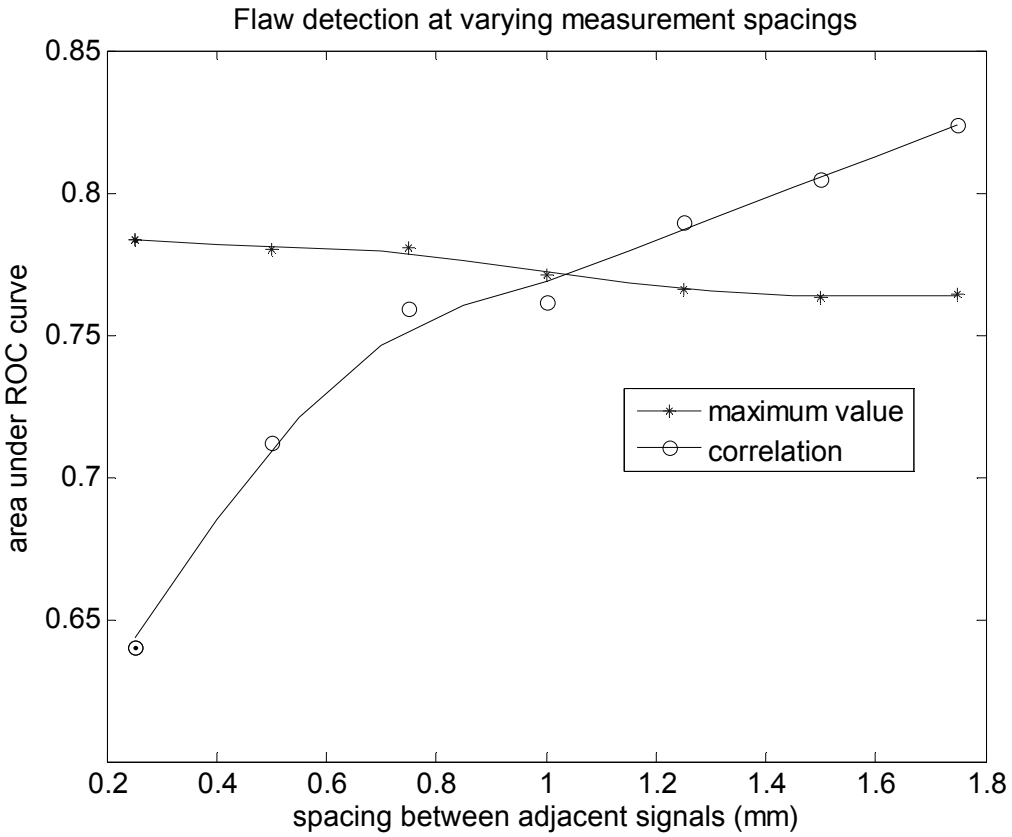

Fig. 4. The area under the ROC curve of the maximum value and correlation statistics as the measurement spacing varies. Signal to noise ratio is held constant at 1.0, flaw size is infinite, and no misalignment, averaging, or realignment is done.

efficacy of both detection statistics increases, but that the relative performance of the correlation statistic is better at low SNR.

The next condition varied was the spacing between adjacent measurement positions. The measurement spacing of the grain noise was varied while the signal to noise ratio was held constant at 1.0. The value of $\tau(i,j)$ was held constant at zero, $B(i,j)$ and $y(i,j,t)$ were held constant over lateral space, and no averaging or realignment was done during analysis. The results are shown in Figure 4. Varying measurement spacing has very little effect on the signals) increases as the measurement spacing decreases because adjacent noise signals are

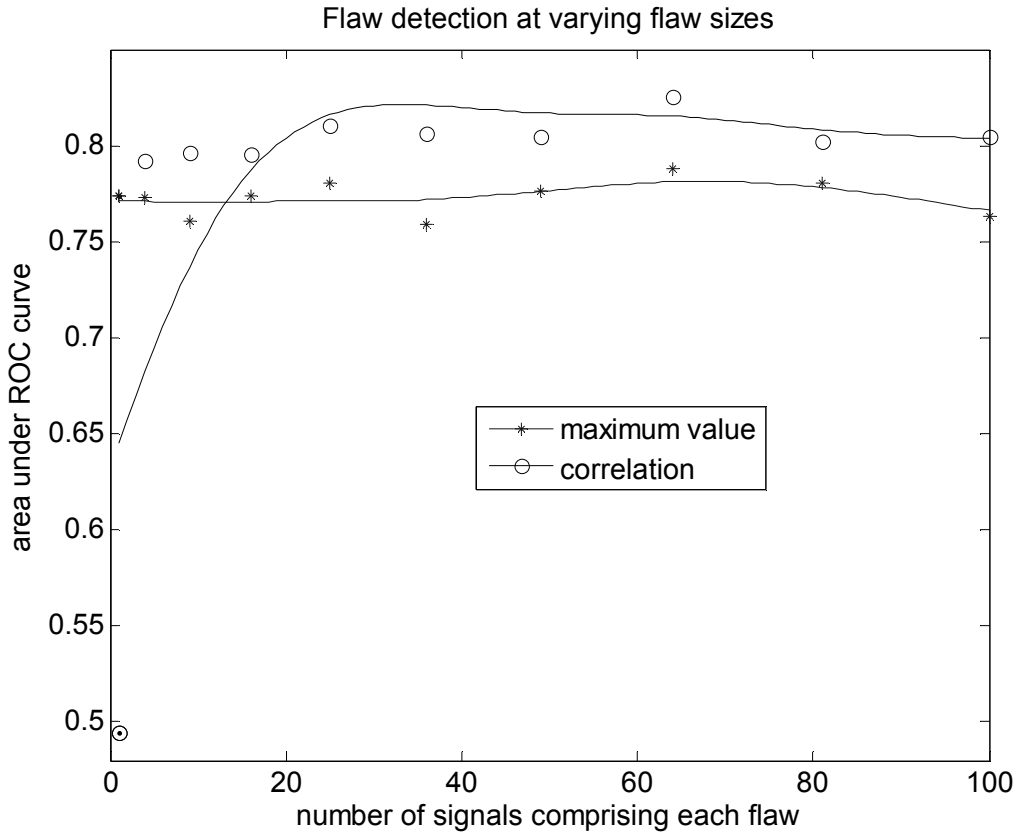

Fig. 5. The area under the ROC curve of the maximum value and correlation statistics as the flaw size increases. Flaw size is indicated on the x-axis as the number of signals collected from each flaw. Measurement spacing is held constant at 1.75 mm, SNR at 1.0, and no misalignment, averaging, or realignment is done.

maximum extreme value, but the efficacy of the correlation statistic as a defect detector increases significantly as the measurement spacing increases. This is explained by the effects of smaller measurement spacing on the correlation noise distribution. The mean of the noise distribution (the distribution of spatial cross correlations between adjacent grain noise more dependent on one another. This increase moves the noise distribution towards the flaw distribution, resulting in less separation between the two and a less ideal ROC curve.

Flaw size is another condition that was varied, and the results for this simulation are shown in Figure 5. To uncouple the results of this simulation from the effects of changes in

measurement spacing, the flaw size was not used for the x-axis, but rather the total number of received A-scans, or signals, indicating a flaw. In this simulation, flaws were created to be square; hence if 25 signals comprise a flaw and the measurement spacing is 1.75, the flaw size can be calculated as being 8.75 mm square. The SNR was held constant at 1.0 and the measurement spacing at 1.75 mm. The value of $\tau(i,j)$ was held constant at zero, $y(i,j,t)$ was held constant over lateral space, and no averaging or realignment was done during analysis. The results for the maximum value do not vary significantly with the number of signals. This is expected since it is necessary for only one A-scan to contain the flaw signal for the MEV statistic to detect a flaw. However, for the correlation statistic to work as a detection method there must be adjacent signals each containing a flaw signal to produce a high correlation, thus flaws are not detected when only one signal is collected from each flaw. Beyond that point, there is no significant variation in the efficacy of the correlation method based on the number of A-scans collected from the flaw.

Spatial averaging is a common image processing technique that increases the probability of detection. Each detection statistic is replaced with the average of itself and a number of its neighbors. This effectively applies low-pass filtering to the image and removes spatial noise, making flaws more easily discerned. Spatial averaging can be applied to any of the detection images as shown in Figure 1. For this simulation, the size of the averaging window was varied from a 1 x 1 window (effectively resulting in no averaging) to a 10 x 10 window (averaging 100 samples in each position), while the SNR was held constant at 1.0, the measurement spacing was 1.75 mm, the value of $\tau(i,j)$ was held constant at zero, $B(i,j)$ and $y(i,j,t)$ were held constant over lateral space, and no realignment was done during analysis. Figure 6 shows the results. Spatial averaging improved the likelihood of detection

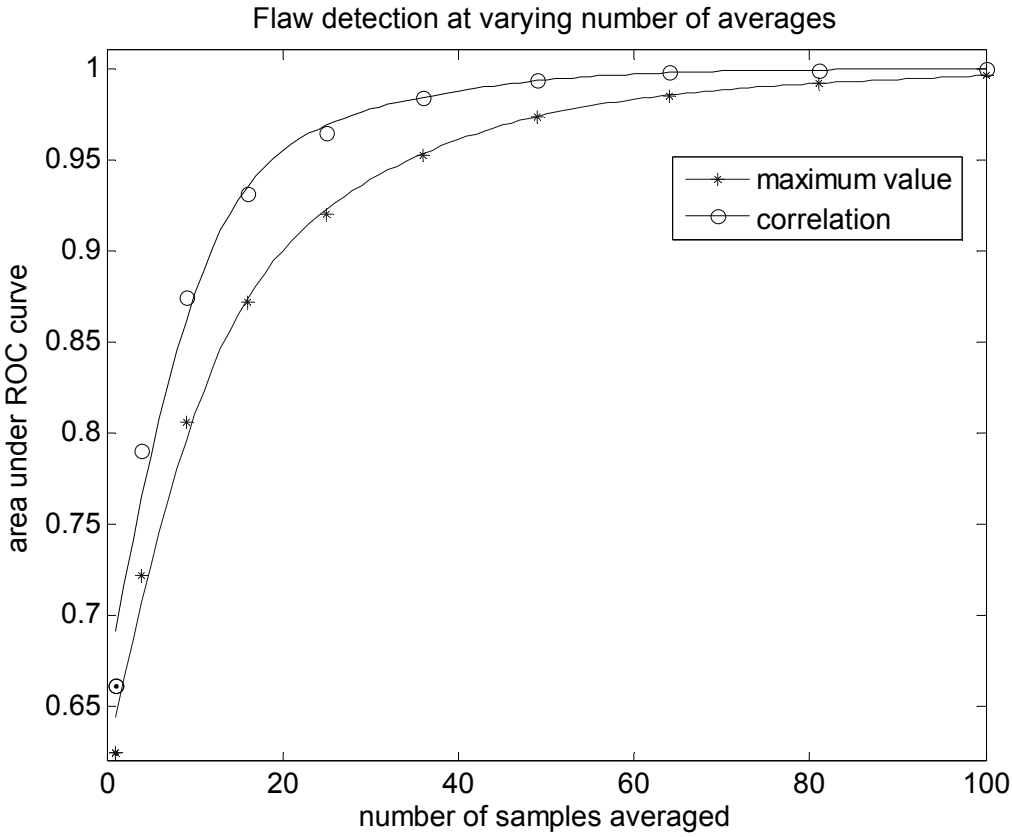

Fig. 6. The area under the ROC curve of the maximum value and correlation statistics as the window size of spatial averaging is increased. Measurement spacing is held constant at 1.75 mm, SNR at 1.0, flaw size is infinite, and no misalignment, or realignment is done.

for both the maximum value and correlation statistic, but did not change their relative efficacy.

It is interesting to note that in Figure 6, the likelihood of detection continues to increase as the number of signals averaged increases. Since a large number of signals were simulated while $B(i, j)$ was held constant over lateral space, the effective flaw size was much larger than the maximum averaging window. In Figure 7, the results of a similar simulation are shown where $B(i, j)$ was set to vary such that the flaw size was 8.75 x 8.75 mm with a 1.75 mm step size, meaning that there were 25 A-scans containing a flaw signal. These results show that the ideal averaging window size is slightly larger than the flaw size.

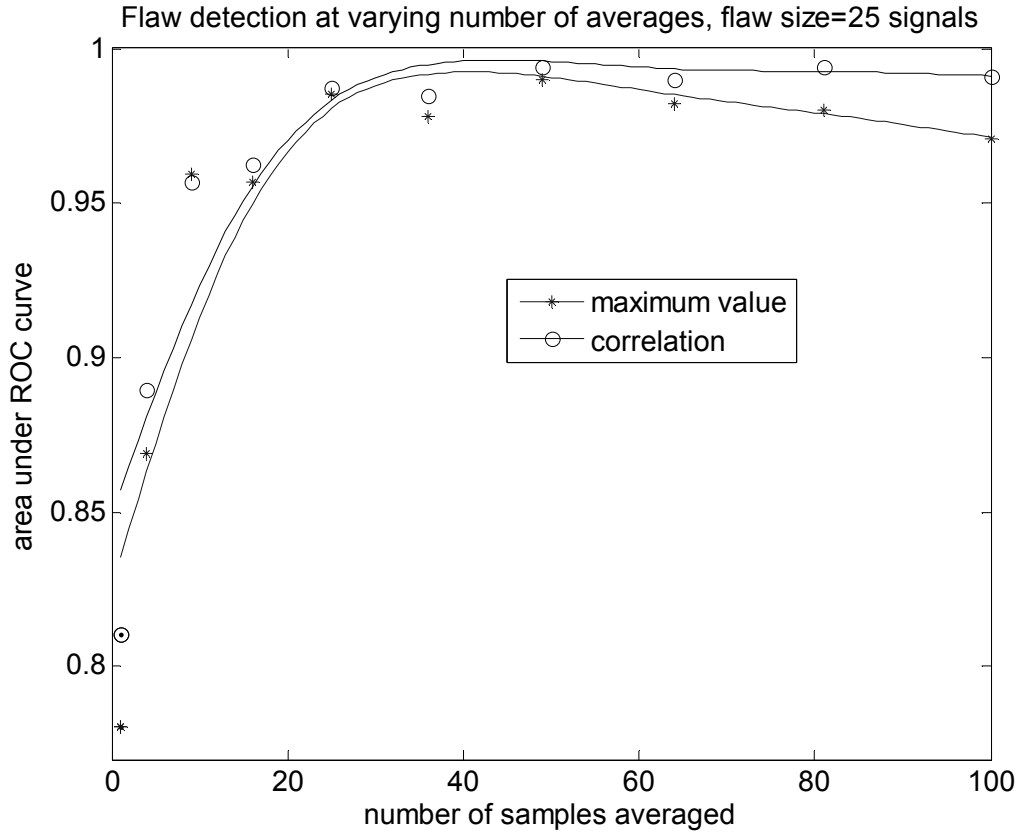

Fig. 7. The area under the ROC curve of the maximum value and correlation statistics as the window size of spatial averaging is increased. In this case, the size of the flaw is 5 x 5, such that 25 signals are collected from each flaw. Measurement spacing is held constant at 1.75 mm, SNR at 1.0, and no misalignment, averaging, or realignment is done.

Beyond this, the likelihood of detection decreases slightly for the spatial correlation statistic, and decreases more significantly for the maximum extreme value statistic.

Misalignment of flaw signals is another issue that changes the efficacy of the correlation detection statistic. An uneven flaw surface can cause the times at which adjacent flaw signals are received to be slightly misaligned, which will reduce the flaw correlation distribution mean. To reduce these effects, one can allow the lag, τ , in Eq. (1) to vary, and the maximum value of the correlation, $\hat{\rho}(\tau)$, will be the detection statistic. To simulate this situation, the flaw signals were misaligned by allowing $\tau(i, j)$ in Eq. (4) to randomly vary

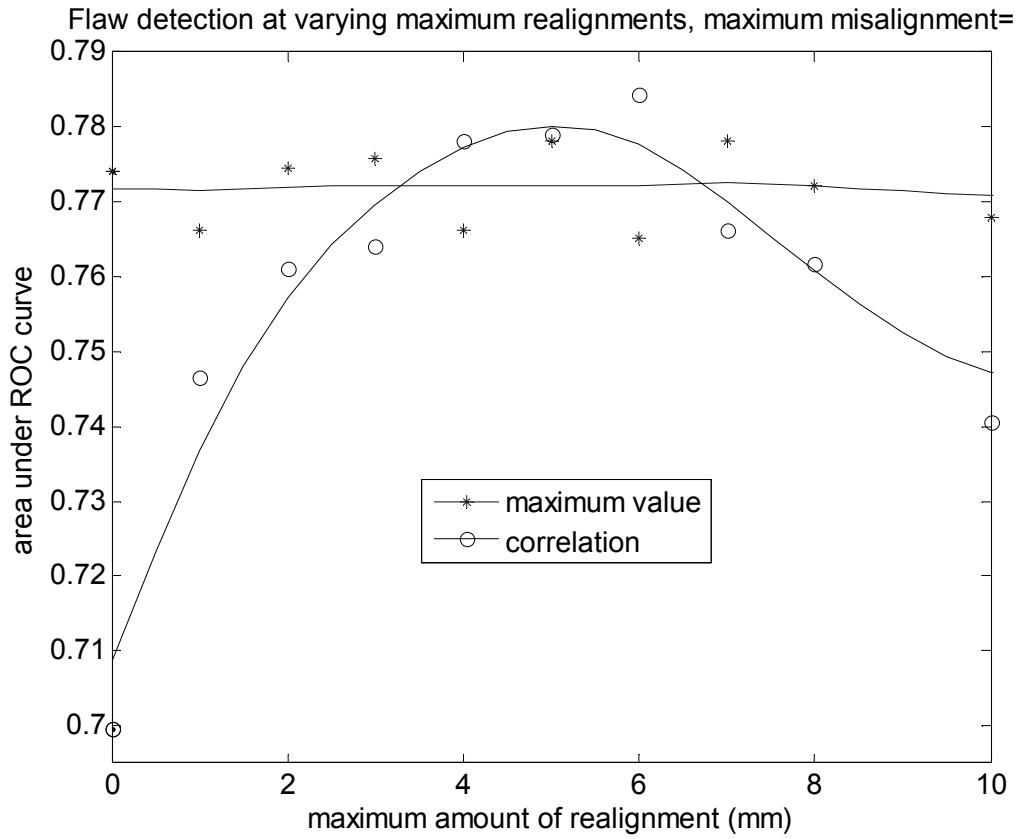

Fig. 8. The area under the ROC curve of the maximum value and correlation statistics as the maximum amount of realignment is increased. In this case, misalignment is randomly applied to the simulated signals such that the maximum number of steps in time that two adjacent signals can be misaligned is 5. Measurement spacing is held constant at 1.75 mm, SNR at 1.0, flaw size is infinite, and no averaging is done.

from -2 to +2 points (which equates to +/-.02 μs). This means that the maximum amount that two adjacent signals could be misaligned from one another was 5 points; assuming one was misaligned by +2 and one by -2. The SNR was held constant at 1.0, the measurement spacing was 1.75 mm, $B(i,j)$ and $y(i,j,t)$ were held constant over lateral space, and no averaging was done. The maximum amount of lag $|\tau|_{\max}$ used in the correlation equation was varied and the results are shown in Figure 8. The variation of the lag has no effect on

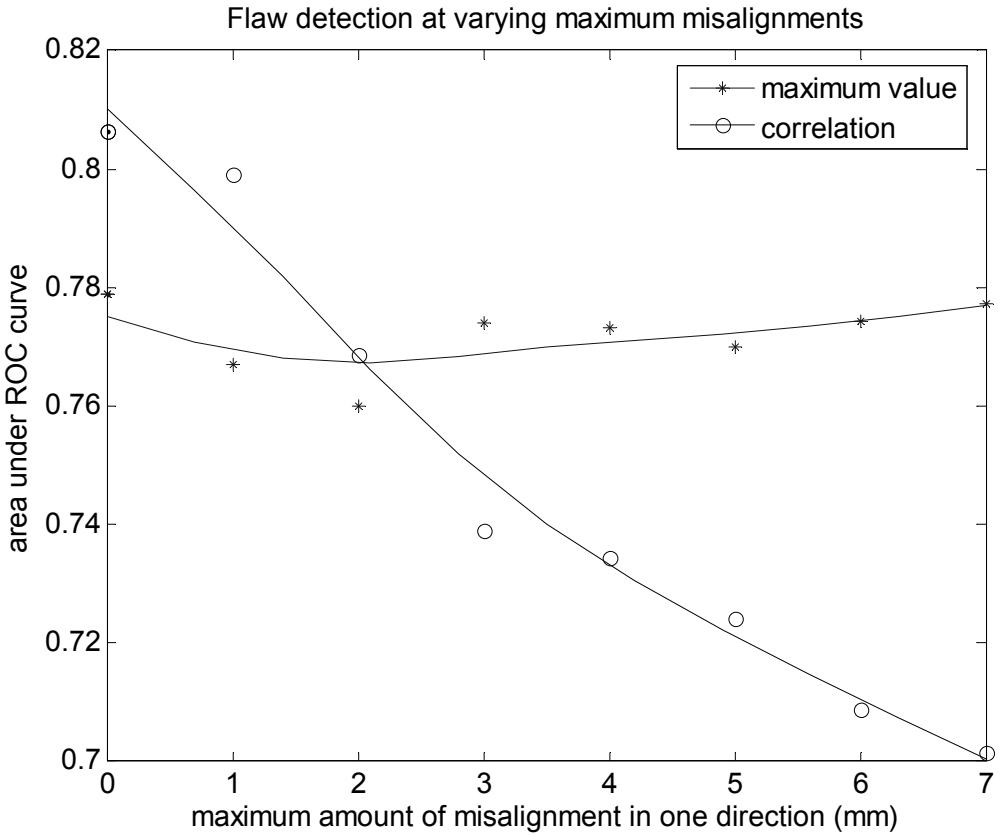

Fig. 9. The area under the ROC curve of the maximum value and correlation statistics as the maximum amount of misalignment is increased. The maximum amount of realignment is set to its ideal value, based on the previous figure. Measurement spacing is held constant at 1.75 mm, SNR at 1.0, flaw size is infinite, and no averaging is done.

the MEV, but the correlation is maximized when $|\tau|_{\max}$ is exactly the maximum misalignment. Beyond this point, the efficacy of the correlation statistic slowly drops.

Figure 9 shows the results for a similar simulation that instead varied the maximum amount of misalignment possible using $\tau(i, j)$, while setting $|\tau|_{\max}$ to be equal to the maximum misalignment possible. The results again show very little effect by the variation on the maximum value statistic, but the efficacy of the correlation statistic drops as the maximum misalignment increases, even when realignment is done to maximize the results. When looking at the individual grain noise and noise corrupted flaw distributions, it can be

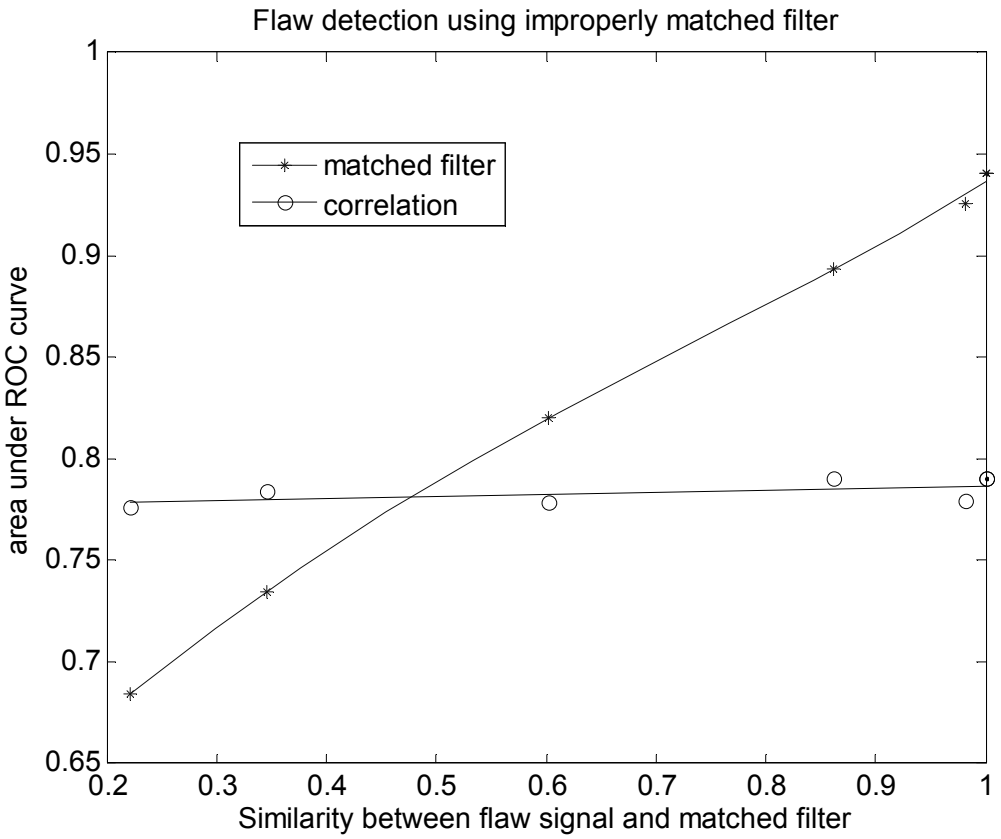

Fig. 10. The area under the ROC curve of the matched filter and correlation statistics as quality of the matched filter template decreases. The quality of the template is plotted on the x-axis as the similarity (or correlation between) the actual flaw signal and the template. Measurement spacing is held constant at 1.75 mm, SNR at 1.0, the flaw size is infinite, and no misalignment, averaging, or realignment is done.

seen that while allowing $|\tau|_{\max}$ to increase such that the mean of the flaw distribution is maximized, it also increases the mean of the noise correlation distribution, creating more overlap between them and a poorer ROC curve.

B. Comparison of Cross-Correlation and Matched Filtering

The spatial cross-correlation detection method was also compared to matched filtering. Matched filtering performs ideally when the expected flaw signal is perfectly known, such that $\alpha_m = 1$. There are many reasons why the chosen matched filter template

might not accurately represent the flaw signal; improperly calculated diffraction and attenuation effects could result in different frequency content from the actual flaw signal, and the actual scattering function of the flaw could significantly change the pulse shape from what is expected. To simulate improperly calculated diffraction and attenuation effects, the matched filter template used, denoted $s_i^m(t)$ in Eq. (3), was varied while the flaw signal, $s_i(t)$, remained the same. The SNR was held constant at 1.0 and the measurement spacing at 1.75 mm. The value of $\tau(i,j)$ was held constant at zero, $B(i,j)$ and $y(i,j,t)$ were held constant over lateral space, and no averaging or realignment was done during analysis. The set of signals used as $y(t)$ for this simulation were the front surface and four subsequent back surface reflections from a copper plate. Each reflection was at a different place in the diffraction field and had a different amount of attenuation. The area under the ROC curve is plotted versus the value of α_m in Figure 10. As can be seen, there is little effect on the efficacy of the correlation coefficient performance. The matched filter template can be somewhat different than the actual flaw signal and the matched filter still performs well, but if the template is significantly different than the actual flaw signal, performance suffers and the correlation coefficient statistic is a better detector.

In some cases, flaws do not produce the same signal over their entire extent, but rather have laterally variable scattering functions. To simulate this situation, the simulation was changed slightly such that the flaw signals, $y(i,j,t)$, were variable over the measurement grid. The data used to simulate this type of flaw were collected from a piece of sandpaper sandwiched between two pieces of Plexiglas. A strong front surface reflection was received from the sandpaper, but the pulse was distorted and the signal varied

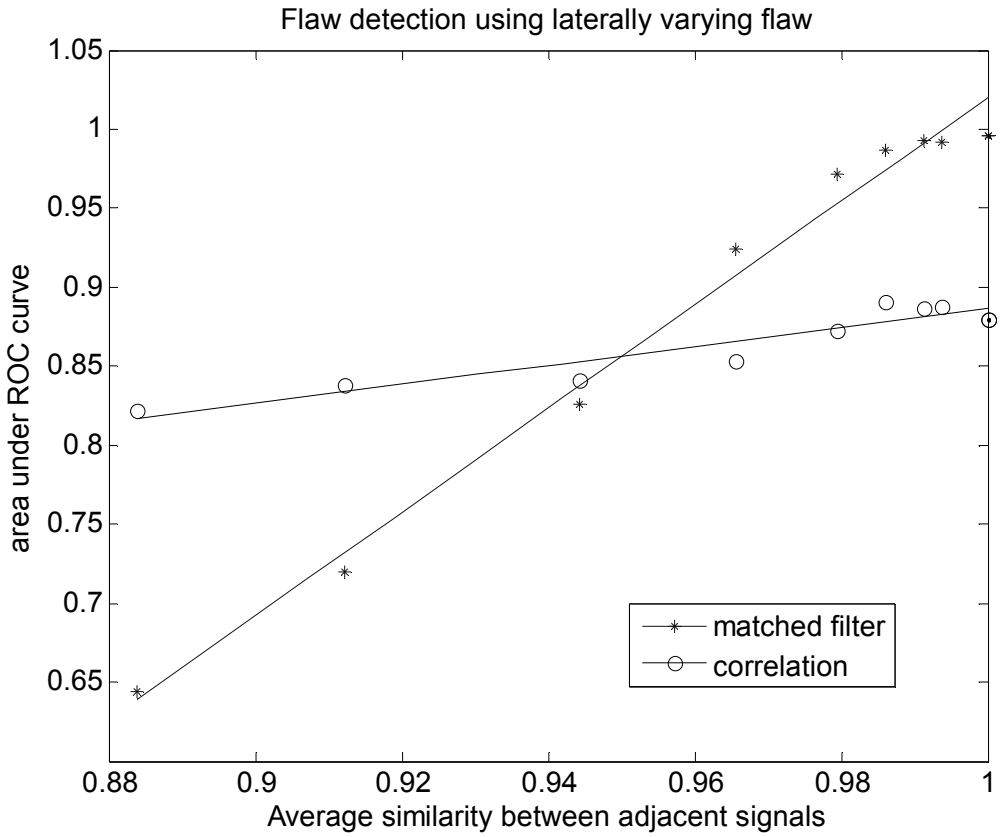

Fig. 11. The area under the ROC curve of the matched filter and correlation statistics as the amount of lateral distortion increases. The lateral distortion is plotted on the x-axis as the average similarity (or correlation between) adjacent flaw signals. Measurement spacing is held constant at 1.75 mm, SNR at 1.0, the flaw size is infinite, and no misalignment, averaging, or realignment is done.

significantly as the transducer moved laterally. The measurement spacing between adjacent signals was increased to simulate a flaw with more lateral distortion. A typical signal from this set was chosen to be used as the matched filter. Figure 11 shows the results of this simulation. In this plot, the x-axis shows the average correlation between adjacent flaw signals before the addition of grain noise, thus in effect measures how quickly the flaw signal changes with lateral space. The increase in lateral distortion (corresponding to a decrease in the average correlation between adjacent flaw signals) reduces the likelihood of detection for

both matched filtering and correlation, but the effect is much more pronounced with matched filtering.

VI. Summary

The use of the spatial cross-correlation coefficient for flaw detection is suggested as an alternative to more commonly used detection statistics under certain circumstances. It must be remembered when interpreting the data presented in this paper that these particular results provide concrete decision points only when all the experimental and analysis variables are similar to those used in these simulations. Because so many variables affect the performance of the correlation coefficient, and because they are likely to vary widely from those presented here, no concrete conclusions can be made about exactly when the spatial cross-correlation statistic should be used as a flaw detection method. However, some general guidelines can be presented, with the caveat that its use should also be evaluated based on the particular experimental conditions.

Generally, the use of the new correlation method should be considered as a complementary analysis technique to gated peak-detection when the signal-to-noise ratio is so low that the performance of the latter begins to suffer. The correlation method has the capability to out-perform gated peak-detection in this case. Additionally, the new correlation method has the capability to outperform matched filtering when an accurate template cannot be determined or when the flaw signal varies widely.

These results also suggest guidelines to be followed when choosing experimental and analysis variables such as measurement spacing, averaging window size, and realignment parameters. The measurement spacing should be chosen to be as large as possible to minimize the average value of the correlation noise distribution, yet still be small enough to

collect more than one signal from each flaw. If spatial averaging is to be applied, the measurement spacing should be such that as many signals as possible are collected from each flaw, while minimizing the average value of the correlation noise distribution. The balance between these conflicting motivations for choosing measurement spacing will need to be determined experimentally based on the particular flaw, material, and transducer characteristics. If flaw surfaces are uneven, resulting in variable times for adjacent flaw signals, the maximum amount of lag will also need to be chosen carefully to account for uneven arrival times without allowing too large of an increase in the distribution of grain noise correlations. Spatial averaging (and likely other image enhancement techniques) can be applied to correlation images, as to C-scan images, and will improve the likelihood of detection in a similar manner for all statistics, but the windowing size must also be carefully chosen based on the number of signals received from each flaw.

Acknowledgements

This work was supported by the Center for Aerospace Manufacturing Technology (CAMT) at the University of Missouri-Rolla funded under Air Force Research Laboratory Contract FA8650-04-C-5704 and by Boeing under PO Z40791. Previous support for development of the correlation approach was provided by Honeywell Federal Manufacturing and Technology and by the National Science Foundation (NSF CMS 9610189). The authors would like to acknowledge early development work on correlation analysis by previous postdocs and students including Dr. Mark D. Russell, Dr. Terence P. Lerch, and Brett Rinker. The authors would also like to acknowledge the tremendous support from personnel at Honeywell FM&T including Eric Jamieson, Jose A. Samayoa, Jason P. Miller and Brett Rinker. In particular,

the encouragement by Eric Jamieson to extent the correlation approach to localized flaw detection was pivotal.

References

1. S. M. Kay, Fundamentals of Statistical Signal Processing Volume II Detection Theory. Prentice-Hall, Upper Saddle River, NJ, 1998.

2. A. D. Whalen, Detection of Signals in Noise, New York: Academic Press, 1971.

3. J. Q. Xin, K. D. Donohue, and N. M. Bilgutay, "Filter design for ultrasonic flaw echo detection in large-grained material", *Review of Progress in Quantitative Nondestructive Evaluation*, Vol. 10A, edited by D. E. Chimenti and D. O. Thompson, Plenum Press, New York, 1991, pp. 725-731.
4. C. P. Chiou, R. B. Thompson, and L. W. Schmerr, "Model-based signal processing techniques for ultrasonic flaw detection: simulation studies", *Review of Progress in Quantitative Nondestructive Evaluation*, Vol. 12A, edited by D. E. Chimenti and D. O. Thompson, Plenum Press, New York, 1993, pp. 703-710.

5. K. Srinivasan, C. Chiou, and R. B. Thompson, "Ultrasonic flaw detection using signal matching techniques", *Review of Progress in Quantitative Nondestructive Evaluation*, Vol. 14A, edited by D. E. Chimenti and D. O. Thompson, Plenum Press, New York, 1993, pp. 711-718.

6. J. S. Bendat and A. G. Piersol, *Engineering Applications of Correlation and Spectral Analysis*, J. Wiley, New York, p. 46, 1993.

7. W. F. Walker, "The significance of correlation in ultrasound signal processing", *Proc. SPIE Vol. 4325, Medical Imaging: Ultrasonic Imaging and Signal Processing*, edited by Michael F. Insana and K. Kirk Shung, 2001, pp. 159-171.

8. B. A. Rinker, E. E. Jamieson, J. A. Samayoa, T. G. Abeln, T. P. Lerch, and S. P. Neal, "Detection of weak interface signals for same material bond/weld inspection", *Review of Progress in Quantitative Nondestructive Evaluation*, Vol. 22B, edited by D. E. Chimenti and D. O. Thompson, AIP, Melville, 2003, pp. 1080-1087.

9. R. Cepel, K. C. Ho, B. A. Rinker, D. D. Palmer, Jr., and S. P. Neal, "Ultrasonic detection using correlation images", *Review of Progress in Quantitative Nondestructive Evaluation*, Vol. 26, edited by D. E. Chimenti and D. O. Thompson, AIP, Melville, 2007, (in press).

10. R. Cepel, K. C. Ho, B. A. Rinker, D. D. Palmer, Jr., T. P. Lerch, and S. P. Neal, "Spatial correlation coefficient images for ultrasound detection", *IEEE Trans. Ultrason. Ferroelectr. Freq. Control* (in press).

11. R. Cepel, L. Thombs, K. C. Ho, and S. P. Neal, "Statistical analysis and computer generation of spatially correlated acoustic noise", *J. Nondestr. Eval*., (in press).

12. R. B. Thompson, L. Yu, and F. J. Margetan, "A formal theory for the spatial correlation of backscattered ultrasonic grain noise", *Review of Progress in Quantitative Nondestructive Evaluation*, Vol. 24, edited by D. E. Chimenti and D. O. Thompson, AIP, Melville, 2005, pp. 1292-1299.

13. A. K. Jawn, "*Fundamentals of Digital Image Processing*", Prentice-Hall, 1989

14. S. M. Kay, "*Fundamentals of Statistical Signal Processing & Detection Theory*", Prentice Hall NJ, 1998

CHAPTER 5
CONCLUSION

The correlation approach outlined in this work is attractive as a potential compliment to the classical C-scan approach for a number of reasons including: the correlation approach is scale independent; the correlation approach relies on signal shape, while the C-scan approach uses only the peak value; correlations are calculated based on same A-scans used in forming C-scan images; the correlation images described here have a qualitatively similar appearance to C-scan images, facilitating inspector acceptance; and correlation images can be formed without the expertise required to deal explicitly with wave propagation and scattering effects.

However, while the correlation approach is amplitude independent, it is not measurement system or material independent. To assess its usefulness in a variety of circumstances, simulation studies were utilized. To ensure the accuracy of the simulations, simulated acoustic noise was created whose correlation coefficient distributions and maximum extreme value distributions match those of measured acoustic noise.

Based on limited simulations, the use of the spatial cross-correlation coefficient for flaw detection is suggested as an alternative to more commonly used detection statistics under certain circumstances. Generally, the use of the new correlation method should be considered as a complementary analysis technique to gated peak-detection when the signal-to-noise ratio is so low that the performance of the latter begins to suffer. The correlation method has the capability to out-perform gated peak-detection in this case. Additionally, the

new correlation method has the capability to outperform matched filtering when an accurate template cannot be determined or when the flaw signal varies widely.

The simulation results also suggest guidelines to be followed when choosing experimental and analysis variables such as measurement spacing, averaging window size, and realignment parameters. The measurement spacing should be chosen to be as large as possible to minimize the average value of the correlation noise distribution, yet still be small enough to collect more than one signal from each flaw. If spatial averaging is to be applied, the measurement spacing should be such that as many signals as possible are collected from each flaw, while minimizing the average value of the correlation noise distribution. The balance between these conflicting motivations for choosing measurement spacing will need to be determined experimentally based on the particular flaw, material, and transducer characteristics. If flaw surfaces are uneven, resulting in variable times for adjacent flaw signals, the maximum amount of lag will also need to be chosen carefully to account for uneven arrival times without allowing too large of an increase in the distribution of grain noise correlations. Spatial averaging (and likely other image enhancement techniques) can be applied to correlation images, as to C-scan images, and will improve the likelihood of detection in a similar manner for all statistics, but the windowing size must also be carefully chosen based on the number of signals received from each flaw.

When interpreting the data presented in this paper, it must be remembered that these particular results are applicable only when all the experimental and analysis variables are similar to those used in these simulations. Because so many variables affect the performance of the correlation coefficient, and because they are likely to vary widely from those presented here, no firm conclusions can be made about exactly when the spatial cross-correlation

statistic should be used as a flaw detection method under dissimilar experimental conditions. Future work on this problem will extend the comparison between the three detection methods, both through more extensive simulations and by further development of the matched filtering and correlation models.